JAERI-M
8198

CONCEPTUAL STUDIES OF PLASMA ENGINEERING TEST FACILITY

April 1979

Toru HIRAOKA, Teruhiko TAZIMA, Masayoshi SUGIHARA,
Masao KASAI,* Kichiro SHINYA** and Hiroki SAKAMOTO***

日本原子力研究所
Japan Atomic Energy Research Institute

この報告書は，日本原子力研究所がJAERI-Mレポートとして，不定期に刊行している研究報告書です．入手，複製などのお問合わせは，日本原子力研究所技術情報部（茨城県那珂郡東海村）あて，お申しこしください．

JAERI-M reports, issued irregularly, describe the results of research works carried out in JAERI. Inquiries about the availability of reports and their reproduction should be addressed to Division of Technical Information, Japan Atomic Energy Research Institute, Tokai-mura, Naka-gun, Ibaraki-ken, Japan.

JAERI-M 8198

Conceptual studies of Plasma Engineering Test Facility

Toru HIRAOKA, Teruhiko TAZIMA, Masayoshi SUGIHARA
Masao KASAI*, Kichiro SHINYA**, Hiroki SAKAMOTO***

Division of Large Tokamak Development
Tokai Research Establishment, JAERI

(Received March 12, 1979)

Conceptual studies have been made of a Plasma Engineering Test Facility, which is to be constructed following JT-60 prior to the experimental power reactor. The physical aim of this machine is to examine self-ignition conditions. This machine possesses all essential technologies for reactor plasma, i.e. superconducting magnet, remote maintenance, shielding, blanket test modules, tritium handling. Emphasis in the conceptual studies was on structural consistency of the machine and whether the machine would be constructed practically.

Key words: Tokamak Reactor, Self-Ignition Conditions, Plasma Engineering Test Facility, Conceptual Studies, Structural Consistency

---

* on leave from Mitsubishi Atomic Power Industry Inc
** on leave from Toshiba Co. Ltd.
*** on leave from Mitsubishi Heavy Industries Ltd.

炉心工学試験装置概念検討

日本原子力研究所東海研究所大型トカマク開発部
平岡　徹・田島輝彦・杉原正芳・笠井雅夫 *
新谷吉郎 ** ・坂本寛己 ***

（1979年3月12日受理）

炉心工学試験装置の概念検討を行なった。この装置はJT－60の次の装置として，実験炉に先立って建設されるものである。その物理的目標は自己点火条件を検証する事である。一方この装置は将来の核融合炉に必要な全ての技術を備えたものである。したがって例えば超電導磁石，遠隔操作技術，遮蔽，ブランケット試験モジュール，トリチウム取扱い技術の確立等が必須となる。この概念検討では予備設計に先立ち，装置が一つの構造体として現実に成り立ち得るかどうかに重点を置いて検討を行なった。

*　三菱原子力工業（株）外来研究員
**　東京芝浦電気（株）外来研究員
***　三菱重工業（株）外来研究員

CONTENTS

目　　次

1. Introduction

Japan Atomic Energy Commission has recognized in 1973 the necessity of a large tokamak machine to follow JT-60 prior to the experimental power reactor in its long range program for development of the fusion reactor. It has been called "Mock-up Test Facility (MTF)" with the aim for the preliminary test of reactor plasma of the experimental reactor.

JAERI initiated the design study of Experimental Reactor (JXFR). Its design was proceeded as a driven-type 100 MW reactor to clarify engineering problems. However, the progress of physics is so aggressive in these several years that its physical scope seems to be a little bit conservative. On the other hand, the energy multiplication factor, Q, more than thirty will be required for future power reactor stations. At the pressure time, it is anticipated that the plasma at the level of $Q \simeq 2$ will be realized in the up-grade phase of the large tokamak generation now under construction. The next physical mile stone in the approach for the tokamak power reactor is to reach or to be close to the self-ignition condition.

From the engineering point of view, the next machine should furnish all essential technologies for maintaining reactor relevant plasma. The technologies concerning to resources such as tritium and real energy multiplication with high duty cycle will be imposed on in the further future machine, that is, Experimental Power Reactor.

Thus, Plasma Engineering Test Facility is defined as the facility to testify both of physical and essential engineering steps by a single machine with relatively low duty cycle. Then, it has a physical scope a little bit beyond JXFR and an engineering scope a little bit below JXFR.

In the following chapters, the conceptual outlines of PETF and the problems at designing are described.

(T. Hiraoka)

2. Summary of PETF

In Table 2.1, the main design parameters of PETF are summarized. The cross sectional and the top schematical view are shown in Figs. 2.1 and 2.2, respectively.

1. Introduction

Japan Atomic Energy Commission has recognized in 1973 the necessity of a large tokamak machine to follow JT-60 prior to the experimental power reactor in its long range program for development of the fusion reactor. It has been called "Mock-up Test Facility (MTF)" with the aim for the preliminary test of reactor plasma of the experimental reactor.

JAERI initiated the design study of Experimental Reactor (JXFR). Its design was proceeded as a driven-type 100 MW reactor to clarify engineering problems. However, the progress of physics is so aggressive in these several years that its physical scope seems to be a little bit conservative. On the other hand, the energy multiplication factor, Q, more than thirty will be required for future power reactor stations. At the pressure time, it is anticipated that the plasma at the level of $Q \simeq 2$ will be realized in the up-grade phase of the large tokamak generation now under construction. The next physical mile stone in the approach for the tokamak power reactor is to reach or to be close to the self-ignition condition.

From the engineering point of view, the next machine should furnish all essential technologies for maintaining reactor relevant plasma. The technologies concerning to resources such as tritium and real energy multiplication with high duty cycle will be imposed on in the further future machine, that is, Experimental Power Reactor.

Thus, Plasma Engineering Test Facility is defined as the facility to testify both of physical and essential engineering steps by a single machine with relatively low duty cycle. Then, it has a physical scope a little bit beyond JXFR and an engineering scope a little bit below JXFR.

In the following chapters, the conceptual outlines of PETF and the problems at designing are described.

(T. Hiraoka)

2. Summary of PETF

In Table 2.1, the main design parameters of PETF are summarized. The cross sectional and the top schematical view are shown in Figs. 2.1 and 2.2, respectively.

Table 2.1 PETF main parameters

Operation		
Expected operation span		10 years
Total number full power		8×10^4
Pulse repetition period		1200 sec.
Burning flat top period		30 - 60 sec.
Peak fusion power		260 MW
Average fusion power (60 sec. burning)		13 MW
Plasma rise time	up to 1 MA	0.5 sec
	up to max.	4.0 sec.
Plasma		
Major radius		6.2 m
Minor radius	vertical	2.1 m
	horizontal	1.4 m
Plasma volume		338 m^3
Elliptical elongation		1.5
Triangularity		0.5
Aspect ratio		4.43
Toroidal field at axis		4.8 T
Plasma current		4.9 MA
Safety factor, q_a		2.5
Average plasma temperature		7 keV
Average plasma density		1.6×10^{20} m^{-3}
Confinement time		5.6 sec
Poloidal beta		3.0
Toroidal beta		4.0 %
Permissible Z_{eff}		1.2
Tokamak System		
Distance from plasma inner surface to the straight part of the inner perimeter of toroidal field coil		1.1 m
Out-most distance of toroidal field coil form the tokamak axis		11 m
Assembly structure		Octant assembly

Anticipated assembly		5 times
Vacuum vessel neutron wall loading		0.5 MWm^{-2}
Total neutron flux at peak		3×10^{14} cm^{-2} sec^{-1}
14 MeV neutron flux at peak		4×10^{13} cm^{-2} sec^{-1}
Total neutron dose		2.6×10^{21} cm^{-2}
Heat load	magnetic limiter plate (with flux swinging)	200 Wcm^{2}
	liner	6 Wcm^{-2}

Plasma Chamber

Vacuum vessel	Stainless steel double-wall structure
Material limiter	Pylolitic carbon or molybdenum
Liner	Pylolitic carbon
Vacuum vessel coolant	He gas
One-turn resistance	0.5 m ohm
Baking temperature	400 °C
Vacuum pumping speed	50,000 l/s for 20 °C N_2
Throughput	5×10^{-4} torr·l/sec

Primary Shield

Material		multi-layer of iron, heavy concrete and lead
Thickness	inner side	60 cm
	other, upper and lower sides	90 cm

Toroidal Field Coil

Maximum field		8.3 T
Superconducting material		NbTi
Number of coils		16
Coil current		20 kA
Total ampere-turn		149 MAT
Stored magnetic energy		15 GJ
Coil shape		D-shape
Coil bore	vertical	10.0 m
	horizontal	6.3 m

Cross section	width	0.9 m
	thickness (outer side)	1.5 m
Current density	cable	20 A mm^{-2}
	over all (inner part)	8 A mm^{-2}

Ohmic Heating Coil

Coil material	Oxygen free copper (Ag-copper)
Location	Outside of toroidal field coils
Coil current	140 kA (maximum)
Maximum ampere-turn	2.8 MAT/coil block
	2.4 MAT/m (central part)
Magnetomotive force	34.4 MAT
Magnetic energy	650 MJ
Current density	10 A mm^{-2} at central coils
Plasma current raising method	Current interruption
Power supply capacity	420 MW
Power supply method	Parallel-series hybrid
Joule loss power	87 MW
Total joule loss	5.2 GJ/shot (60 sec. burning)
Flux swing	75 Vsec (double swing)

Control Coil

Coil material	Oxygen free copper (Ag-copper)
Control method	Hybrid type
Location	Outside of toroidal field coils
Number of coil blocks	10
Maximum ampere-turn	5.0 MAT
Maximum magnetomotive force	30 MAT
Stored magnetic energy	1.5 GJ
Power supply capacity	995 MVA
Total joule loss	14.7 GJ

Magnetic Limiter	
Type	Poloidal limiter at the top and the bottom with flux line swinging
Location of coil	Outside of vacuum vessel
Total ampere-turn	3.6 MAT/limiter
Heat load on limiter plate	200 W cm^{-2}
Secondary Shield	
Material	Concrete
Thickness	1.5 m
Tritium	
Inventory	80 gr.
Estimated annual consumption	120 gr. for 30 sec. burning
Neutral Beam Injector	
Injection power	50 MW
Number of port	8
Beam particle	D^+
Injection energy	200 keV
Extracted current	1700 A
Number of ion sources per port	4 (2 × 2 array)
Port cross section	50 cm (width) × 100 cm (vertical)
Net power efficiency	about 30 %
neutralization efficiency	about 20 %
direct recovery efficiency	85 %
Power supply capacity	170 MW
Pumping speed per port	about 10^6 1/sec
Throughput per port	about 100 torr·1/sec

Fig. 2.1 SCHEMATIC CROSS SECTION OF PETF

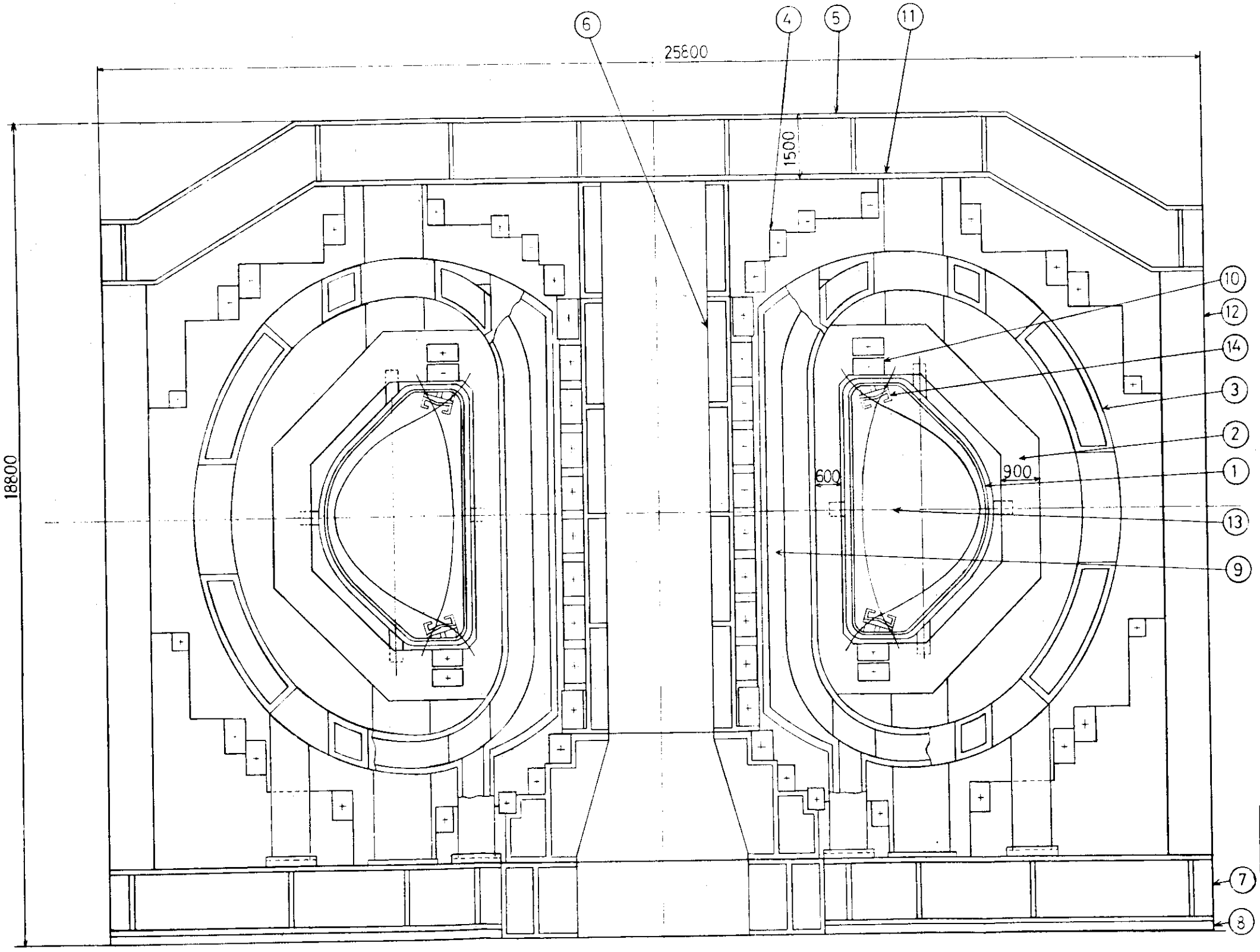

No.	ITEM	NUMBER
11	MAGNETIC LIMITER PLATE	1 set
13	PLASMA	
12	PERIPHERAL STRUCTURE	16
11	SUPERSTRUCTURE	1 set
10	MAGNETIC LIMITER COIL	4
9	CENTRAL CYLINDER	1
8	AIR PAD CASE	8
7	MOVABLE BASE	8
6	CENTRAL COLUMN	1
5	SECONDARY SHIELD	1
4	OH COIL	13
3	TOROIDAL FIELD COIL	12
2	PRIMARY SHIELD	1
1	VACUUM VESSEL	1

Fig. 2.1
SCHEMATIC CROSS
SECTION OF PETF

三角

日本原子力研究所

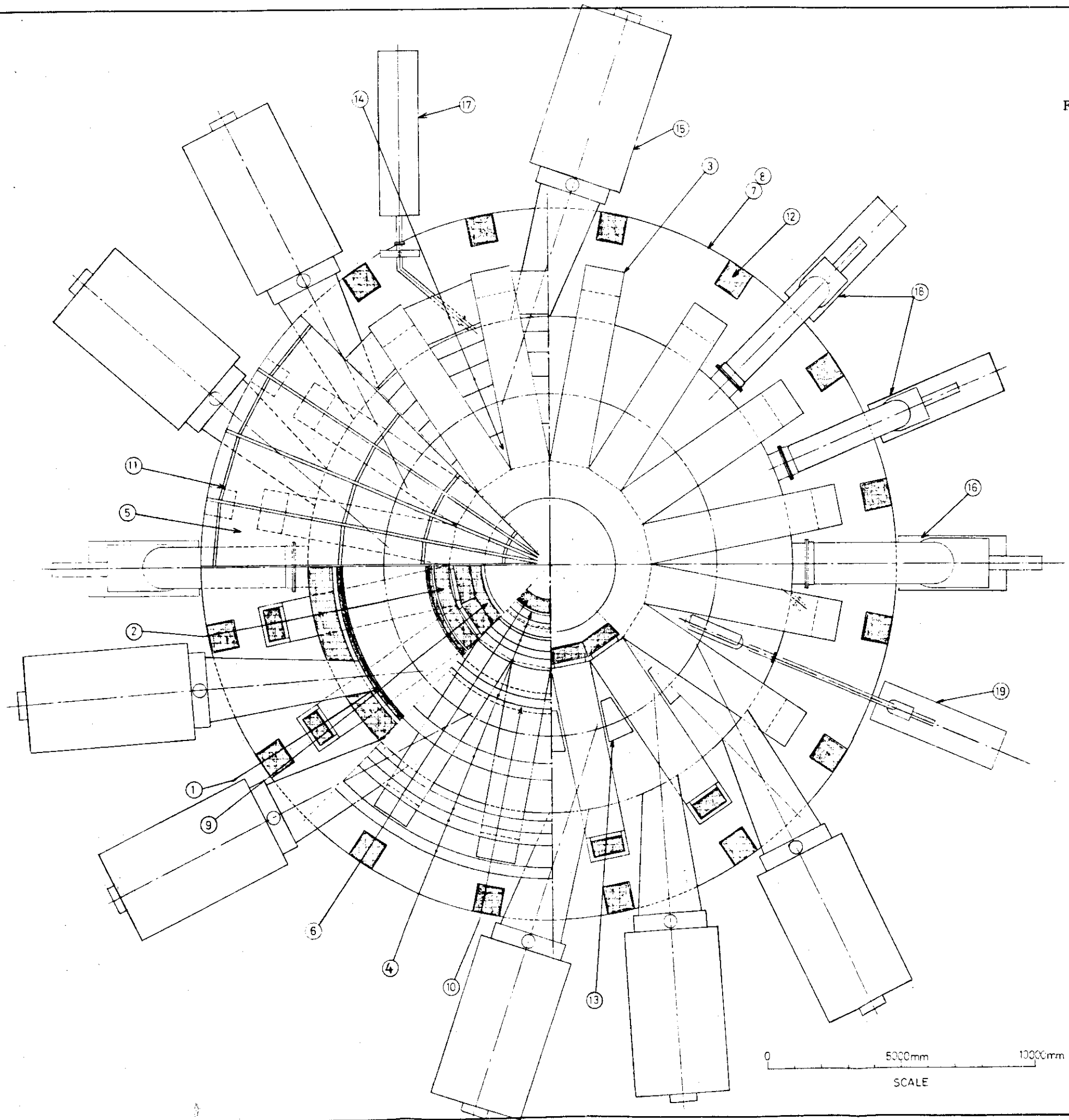

Fig. 2.2 SCHEMATIC TOP VIEW OF PETF

No.	ITEM	NUMBER
19	LASER OSCILLATOR & DETECTOR	1
18	LASER DETECTOR	2
17	LASER OSCILLATOR	1
16	CRYOGENIC PUMP	2 Sets
15	NEUTRAL BEAM INJECTOR	8
14	SUPPORT BETWEEN T.F. COILS	96
13	LEG OF PRIMARY SHIELD	16
12	PERIPHERAL STRUCTURE	16
11	SUPER STRUCTURE	1 Set
10	MAGNETIC LIMITER COIL	4
9	CENTRAL CYLINDER	1
8	AIR PAD CASE	8
7	MOVABLE BASE	8
6	CENTRAL COLUMN	1
5	SECONDARY SHIELD	1
4	OH COIL	13
3	TOLOIDAL FIELD COIL	12
2	PRIMARY SHIELD	1
1	VACUUM VESSEL	1

Fig. 2.2 SCHEMATIC TOP VIEW OF PETF

日本原子力研究所

3. Objectives of PETF and its Development Schedule Plan

Three large Tokamak machines, JT-60, TFTR and JET are now under construction aiming realization of the break even condition. The next and final physical target is to reach the self-ignition condition. On the other hand, there are several essential technologies for development of the tokamak reactor, such as superconducting coil technology, tritium technology and remote handling. We will face the new phase of technological development.

Recently, PLT of Princeton Plasma Physics Laboratory succeeded in reaching the central plasma ion temperature up to 5.5 keV without unstable phenomena although collisionless plasma deeply entered the region of the trapped ion mode region. The energy confinement time still obeys the experimental ALCATOR scaling at $\tau_E \propto \sqrt{q_a}\ \bar{n}\ a^2$ similarly to other existing tokamak machines.

The proportionality coefficient for the experimental scaling at PLT can be expected to be improved by the factor of two at JT-60 by some countermeasure against impurity contamination. Thus, the results of PLT encourages JT-60 to realize one of its targets of $\tau_E \simeq 0.5 \sim 1.0$ sec. If it is accomplished, the possibility to reach the self-ignition condition at the next generation machine will be very high with the realistic machine size.

However, tokamak plasma physics at sufficiently high temperature for dominant fusion reactions and burning control is still remained to be examined in future experiments. Therefore, at the present stage, we had better initiate design work with the plasma parameters reduced from the experimental ALCATOR scaling aiming to reach the self-ignition condition and put emphases in designing on the integrated test of essential relevant plasma engineering to create the reactor plasma such as superconducting magnet or tritium technologies at a single realistic size machine.

By this machine, the reactor relevant plasma engineering such as impurity control or long D-T burning control should be established and all technologies to realize it should be reliably integrated.

The most serious restriction for the next generation machine is cost. The first priority should be put on the effort to keep it as low as possible.

The Long Range Plan for Development of Nuclear Power settled by Japan Atomic Energy Commission in September, 1978, defines the development of PETF as "PETF should be studied aiming its completion within 15 years at

the latest. The machine is supposed to be a tokamak at the present time and it must contribute to the thermonuclear fusion reaction experiment (D-T burning experiments) as a pre-stage for the experimental reactor and to the integrated test of plasma engineering". From the present status of physics and engineering,it sounds reasonable.

PETF many be summarizingly identified in another frank expression as follows:

From the present knowledge of plasma physics, there is high possibility to reach self-ignition condition with the tokamak machine of realistic size restricted by available funding. However, since more definit physical informations to affirm it will be available from JT-60 experiments, the objectives of PETF are focused on the establishment of the essential plasma engineering for future reactor development. Then, if happily possible, the realization of the self-ignition condition will come up into the scope of PETF.

There are two different opinions about the approach to the next generation machine. One of them defines it as the next direct step to the future tokamak reactor and expects to reach the self-ignition condition or to approach close to it and to perform the integration of the essential technologies by the single machine. The other insists to separate the roles of realization of the self-ignition condition and engineering proof such as superconducting coil technology by plural machines and to construct them simultaneously or in series.

The scope and objectives of PETF stand on the former opinion. It seems quite difficult to construct two costly machines simultaneously from budget availability. If they are constructed one after the other, it will take very long time and it will be impossible to keep the final target of proof of nuclear fusion power by a proto-type reactor by 2010's. Therefore, PETF was defined as a machine which can promote both physical and engineering developments to the future tokamak reactor.

The first big step along the development schedule toward the tokamak reactor was made by construction of JT-60. As the second step, Plasma Engineering Test Facility should be accomplished for the definite prespective about realization of fusion power in the beginning of the next century. Japan Atomic Energy Commission has settled the accomplishment of PETF, hopefully by 1990 and by 1994 at the latest in its long range development schedule.

On the other hand, for successful PETF, experiences at design and construction of JT-60 are essential and the research and development for PETF will take longer period than those for JT-60. Thus, allowable period for development of PETF is likely shortened.

The Figure 3.1 shows the plan of PETF development schedule. The basic and universal technologies such as the superconducting magnet or tritium handling will take long period of time for their development and they should be initiated as early as possible. The research and developments which are strongly dependent on the machine design will be initiated after the primary preliminary design. Then, the programs of the research and development are paralelly proceeded with the design works. The main research and developments are supposed to be accomplished prior to the start of construction.

(T. Hiraoka)

Fig. 3.1 PETF DEVELOPMENT SCHEDULE PLAN

JAERI

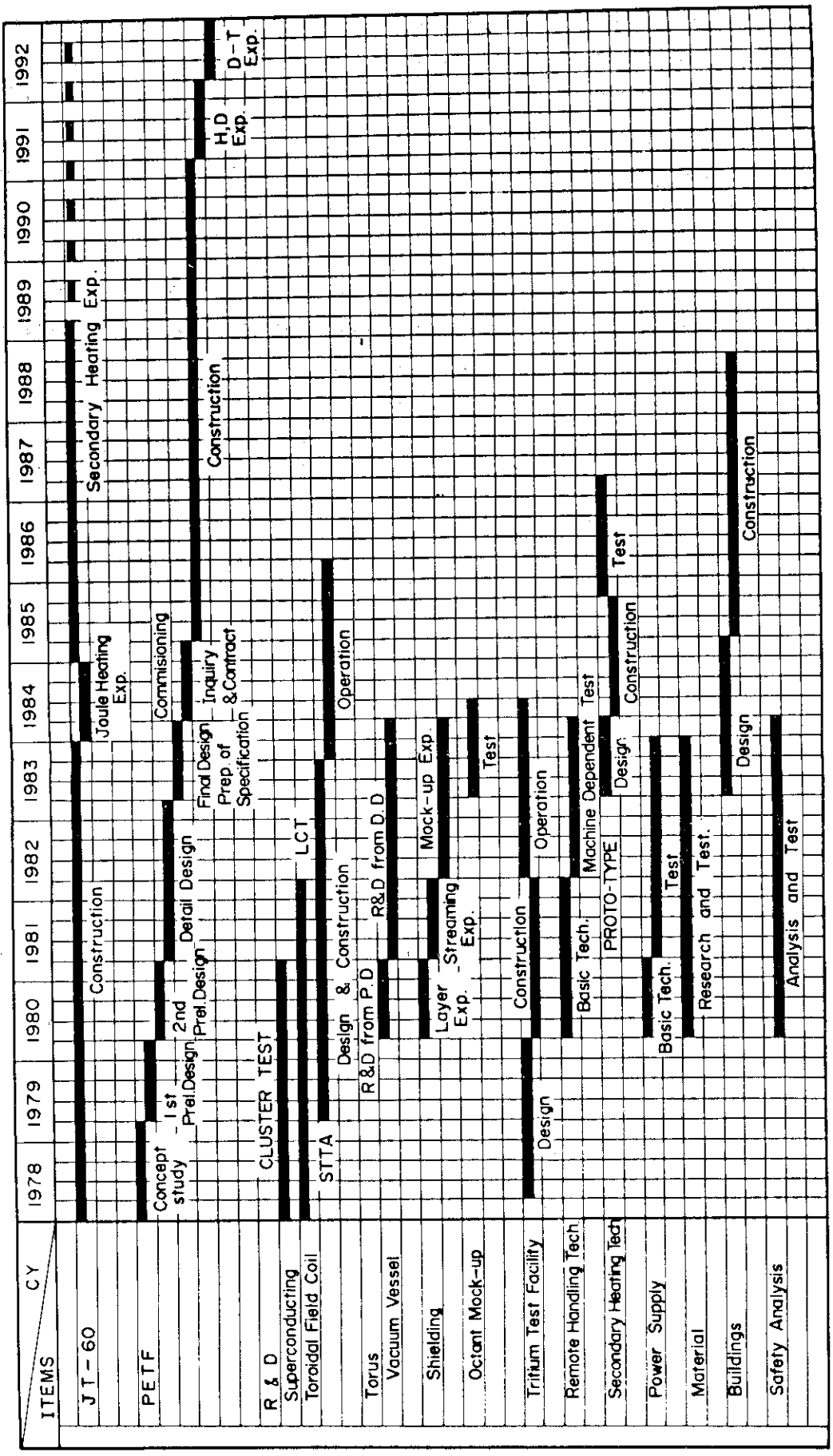

4. Physical Considerations

4.1 Introduction

In determining the plasma and device parameters which enable us to examine the ignition condition, the following three major criteria must be investigated; (1) confinement scaling laws, (2) additional heating, (3) impurity control.

1) Confinement Scaling Laws

Present empirical scaling laws (Alcator scaling law) give rather pessimistic predictions to the future large tokamaks, unless they are improved by at least a factor of 2. When they are thus improved, we can expect several seconds of τ_E at most, but it will be difficult to attain several tens of second under the technological and cost restrictions.

2) Additional Heating

Accordingly, large heating power will be necessary to overcome poor τ_E. However, extremely large power of above 100 MW cannot be expected in PETF. Therefore, a plasma temperature of 7 $\sim$ 10 keV seems to be attainable because of available τ_E value, realistic heating power and expectable α-particle heating power.

Among the additional heating methods, what can be designed realistically at present is the neutral beam injection using positive ions. Not so high beam energy, probably less than 200 keV, is desirable to obtain the required heating power. Thus, excessively large minor radius and high plasma density must be excluded in order to avoid the surface heating of the plasma.

3) Impurity Control

Impurity control sill becomes much more serious problem in the future large tokamaks. It is because neutral beam injection heating power per unit volume decreases as the device size becomes large or the plasma density becomes high, while the energy loss per unit volume due to impurities does not depend on the device size for the same impurity concentration. Furthermore, since the plasma temperature will be raised and the discharge time will be prolonged, the sputtering and the evaporation of

the limiter and first wall materials will inevitably be increased. Therefore, unfortunately we cannot help to employ the poloidal magnetic limiter to avoid the evaporation and to shield the impurity influx.

In addition, as practical problems, it is important to take account of the technological and cost restrictions in determining the plasma and device parameters. In the present design study, we have principally pursued the compactness of the device, retaining the possibility to attain the ignition condition.

4.2 Scaling Laws

A number of empirical[1~3] and theoretical scaling laws[4] have been proposed. It is uncertain, however, that which scaling law can be extended to higher temperature plasma. In the present design study, we employ $\bar{n}\ a^2$ scaling law, expecting its improvement by a factor of 2 and determine the plasma and device parameters. The results are shown in Table 4.1.

4.2.1 $\bar{n}\ a^2$ scaling law[1]

Among many empirical scaling laws proposed so far, the $\bar{n}\ a^2$ scaling law, first proposed by Alcator group, was found to reproduce experimental results obtained in a number of currently operating tokamak devices. There are several ways of describing this scaling law depending on light impurity concentration. One of the expressions for the energy confinement time τ_E by this scaling law can be written as follows.

$$\tau_E = c_s\ \bar{n}\ a_\ell^2 \qquad \text{(s)} \quad . \tag{4.1}$$

Here, $\bar{n}$ abd a_ℓ are average plasma density and the limiter radius of the device, respectively. Proportional coefficient c_s is evaluated to be $(2\sim5)\ \sqrt{q_a} \times 10^{-21}$ in the present day devices, where q_a is the safety factor at the plasma boundary. This coefficient is known to vary depending on the light impurity connection.

Another expression for $\bar{n}\ a^2$ scaling law can be given as

$$\tau_E = 1.5 \times 10^{-20}\sqrt{q_a}\ \bar{n}\ a_{half}^2 \quad \text{(s)} \ , \tag{4.2}$$

where a_{half} is the plasma radius at which the electron temperature is a

half of its center value. In this expression, the influence of impurities on τ_E is implicitly reflected in a_{half}.

The $\bar{n}\, a^2$ scaling law provides the energy confinement time taking account of all of the energy loss (i.e. energy loss due to transport and impurities). When the effects of impurities are diminished, this τ_E will reduce to the one which is evaluated by the transport energy loss only. In the future tokamaks, the effects of impurities must be suppressed sufficiently, as will be discussed later. Therefore, we can assume τ_E given by Eqs. 4.1 and 4.2 to be the one determined by the transport energy loss only.

The total energy confinement time τ_E is defined as

$$\tau_E = \frac{(T_e+T_i)\tau_{Ei}\tau_{Ee}}{\tau_{Ei}T_e + \tau_{Ee}T_i} \quad ,$$

where τ_{Ee} and τ_{Ei} are the electron and ion energy confinement time, respectively. In the present day tokamaks, $\tau_{Ei} \gg \tau_{Ee}$, so that $\tau_E \sim \tau_{Ee}$ $(1 + \bar{T}_i/\bar{T}_e)$. Since $\bar{T}_e > \bar{T}_i$ in joule heated plasma, τ_E given by Eqs. 4.1 and 4.2 is almost equal to τ_{Ee}. In future higher temperature plasma heated by neutral beam injection or α-particles, $\bar{T}_i > \bar{T}_e$, so that $\tau_E \gtrsim 2\tau_{Ee}$. Thus, we can expect that τ_E given by Eqs. 4.1 and 4.2 can be improved by about a factor of 2 in future plasmas. (see Ref. (23) in detail)

4.2.2 Trapped particle mode scaling laws

A transport theory predicts that the trapped particle instabilities will be excited in the future tokamak plasmas of higher temperature and that they will determine the energy loss in these plasmas[4]. Of these instabilities, in the parameter range of PETF, the dissipative trapped ion and electron instabilities will be most dangerous. The scaling lows by these instabilities are given as[5]

(a) Trapped Ion Mode Scaling

$$(\bar{n}\ \tau_E)_{TI} = c_{TI}\ (\frac{1+K^2}{2})^2\ \frac{\beta_{pe}^2 Z_{eff}\ a^4\ B_t^6\ \ell n\Lambda (1+\tilde{T})^2}{q_a^4\ A^{3/2}\ \bar{T}^{11/2}} \quad (m^{-3}\cdot s), \quad (4.3)$$

(b) Trapped Electron Mode Scaling

$$(\bar{n}\ \tau_E)_{TE} = c_{TE}\ (\frac{1+K^2}{2})^2 (\frac{a\ B_t}{q_a})^2\ \frac{\bar{T}^{1/2}}{Z_{eff}\ A^{3/2}} \quad (m^{-3}\cdot s)\ . \quad (4.4)$$

Notations used in these expressions are as follows;

a : plasma minor radius (m),

A : aspect ratio,

B_t : toroidal magnetic field on axis (T),

β_{pe}: poloidal beta value of electrons,

K : ellipticity

Z_{eff}: effective charge,

$\bar{T}$: average temperature,

$\ell n\Lambda$: coulomb logarithm,

$\tilde{T} = \bar{T}_e/\bar{T}_i$.

Numerical coefficients c_{TI} and c_{TE} predicted by theories may have ambiguities of an order of magnitude.

4.2.3 Choice of scaling law

It has been considered that $\bar{n}\ a^2$ scaling law can be applied only to the plasma in joule heating regime. However, the recent experiments of PLT[6], in which the temperature of several keV has been attained by neutral beam injection (NBI) heating, show that $\bar{n}\ a$ scaling law is still applicable even to the plasma in the regime of trapped particle instabilities. In these experiments, $P_h > P_j$ and $\nu_i^* \lesssim 0.1$ (P_h: NBI heating power, P_j: joule heating power, $\nu_i^* = \nu_{ii}^{eff}/\omega_{bi}$: ion's collisionality, where ν_{ii}^{eff} is the effective ion collision frequency and ω_{bi} is the ion bounce frequency), and the trapped particle instabilities are not excited. Thus, $\bar{n}\ a^2$ scaling law may be extended even to higher temperature plasma in the future large tokamaks. However, when c_s takes smaller value (i.e. $2\sqrt{q_a} \times 10^{-21}$), Eq. 4.1 will require considerably large device parameters. In order to attain the self-ignited state in a realistic sized device, the coefficient c_s need take larger value (i.e. $\sim 5\sqrt{q_a} \times 10^{-21}$). Further improvement can possibly be performed by broadening the electron temperature distribution. We can expect the effect of large plasma radius, and besides we should control impurity concentration and additional heating deposition.

If the trapped particle instabilities are excited as predicted theoretically, it seems to be quite difficult to attain the self-ignited state in a realistic sized device[7]. Especially, the temperature dependence of τ_E by the trapped ion mode scaling (i.e. $\tau_E \propto T^{-7/2}$) is quite stringent for temperature rising. In fact, in order to raise the temperature by 50%, an order of magnitude larger heating power is required.

Both $\bar{n}\ a^2$ and trapped particle mode scaling laws have certain ambiguities in their numerical coefficients as mentioned above. It is one of the principal purposes of near future large tokamaks such as JT-60, TFTR, JET and T-15, which are now under construction, to diminish these ambiguities.

In the present design study, we will employ the $\bar{n}\ a^2$ scaling law in principle, by which the total energy confinement time τ_E is given as

$$\tau_E = 1.1\ \sqrt{q_a} \times 10^{-20}\ \bar{n}\ a_\ell^2 \quad . \tag{4.5}$$

This τ_E is the best one, which has been obtained so far, with further slight improvement. This improvement can be achieved when $a_{half} \sim 0.6\ a_\ell$ and $q_a = 2.5$ in Eq. 4.2. The parabolic distribution of electron temperature is sufficient to meet this requirement. Using Eq. 4.5, we will determine the device and plasma parameters to examine the self-ignition condition. We will also investigate, under what values of the coefficients c_{TI} and c_{TE}, this device can examine the self-ignition condition when trapped particle mode scalings are applied.

4.3 Plasma and Device Parameters

4.3.1 Self-ignition condition

The self-ignition condition is given as

$$P_r + \frac{3\ \bar{n}\ k\ \bar{T}}{\tau_E} = \frac{1}{4}\ \bar{n}^2\ \langle\sigma v\rangle_f\ E_\alpha\ , \tag{4.6}$$

where P_r, E_α and $\langle\sigma v\rangle_f$ are radiation energy loss, the energy of α-particle and the D-T thermonuclear reaction rate averaged over a Maxwellian energy distribution, respectively. We will take account of bremsstrahlung radiation loss for P_r given as

$$P_r \equiv P_B = 1.5 \times 10^{-38}\ \bar{n}^2 \sqrt{\bar{T}}\ Z_{eff} \qquad (W/m^3)\ . \tag{4.7}$$

Before determining the plasma and device parameters by using Eqs. 4.1, 4.5, 4.6 and 4.7, we will discuss the plasma shape, aspect ratio and ignition temperature in the following sub-sections.

4.3.2 Plasma shape

We adopt non-circular plasma to raise beta value. Among various shapes of non-circular plasmas such as ellipse, D-shape, doublet shape and so on, numerical calculations show that D-shape plasma is superior to other shapes in the stability for localized interchange modes near the rational surface.[8] Thus, in the present design study, we will adopt D-shape plasma. According to Ref. (8), the maximum critical beta value can be obtained when the ellipticity $K \sim 1.65$ and the triangularity $\delta_t \sim 0.5$. We will set $K = 1.5$ and $\delta_t = 0.5$, in order to avoid excessively large size of the device.

Note that, up to this time, it has been made clear only for the localized interchange mode that D shape is superior to other shapes and that the maximum critical beta value can be obtained at such values of K and δ_t. The beta value criteria for the ballooning mode, which is localized near the bad curvature region of the torus, are now under investigation. Another optimum shape and critical beta value will also be possible by further theoretical and experimental investigations on high beta plasma.

4.3.3 Aspect ratio and temperature

In order to examine the dependence of the device parameters on aspect ratio and temperature, we rewrite Eq. 4.6 in the following form by using Eqs. 4.5 and 4.7.

$$1.5\times10^{-38}\, Z_{eff}\sqrt{\bar{T}} + \frac{3\,k\,\bar{T}^3}{1.8\times10^{-20}a^2}\,\frac{(4\mu_0 k)^2}{\beta_p^2}\,\frac{1}{B_t^4}\left(\frac{q_a^2A^2}{f(K)}\right)^2 = \frac{1}{4}\,\langle\sigma v\rangle_f\, E_\alpha, \tag{4.8}$$

where f(K) represents the non-circular effect. For simplicity, we use the following form for f(K),

$$f(K) = (1 + K^2)/2 \quad , \tag{4.9}$$
$$K = b/a \quad ,$$

which corresponds to the elliptical cross section of the plasma. The toroidal magnetic field at plasma axis B_t is given as

$$B_t = B_{max}\left(1 - \frac{1 + \Delta/a}{A}\right) \quad , \tag{4.10}$$

where B_{max} and Δ are the maximum field at the inner perimeter of D-shaped coil and the distance between the inside surface of plasma and the straight part of the inner perimeter of D-shaped toroidal coil, respectively. Smaller Δ is desirable to strengthen the magnetic field at the plasma. Considering, however, the spaces for the double-walled structure of the vacuum vessel, shielding materials and the cryostat for superconducting toroidal magnet, Δ of at least 1.1 $\sim$ 1.2 meter will be required. On the other hand, the development of NbTi superconducting toroidal magnet seems to be most promissing at present. We can expect to obtain 8 tesla for B_{max} by this magnet. The development of Nb_3Sn coils is rather behind that of NbTi coils. Stronger field (B_{max} of 12T) will be obtained by Nb_3Sn superconducting magnet.

Figure 4.1 shows the temperature dependence of the required plasma minor radii a_{ig} derived from Eqs. 4.8, 4.10 so as to attain the self-ignited state. As can be seen from this figure, a_{ig} depend on the temperature very weakly, and have their minima near 9 keV. No remarkable changes of a_{ig} can be recognized in the temperature region of 7 $\sim$ 10 keV. Thus, in order to avoid the difficulties of the additional heating, as will be discussed later, rather low temperature of about 7 keV seems to be more advantageous for the target temperature.

The curve (a) in Fig. 4.2 shows the aspect ratio dependence of a_{ig}, when $\bar{T}$ is 7 keV. The minimum value of a_{ig} can be obtained when A $\sim$ 5.5. From the view point of the device size, such a large aspect ratio can not be preferable, since a capacity of power supply as well as a plasma volume will become quite large. If we choose a plasma volume as a measure of compactness, the plasma volume for the self-ignited plasma takes its minimum value when A $\sim$ 4, as is shown by the curve (b) in Fig. 4.2.

From the above discussion, we will set the target temperature $\bar{T}$ of about 7 keV and the aspect ratio A of about 4.5.

4.3.4 Design value by $\bar{n}\, a^2$ scaling law

As has been discussed in the preceding section, the development of superconducting toroidal magnet in near future seems to be promissing for NbTi coil at present. Furthermore, τ_E given by $\bar{n}\, a^2$ scaling law, is not affected by B_t explicitly, as long as the beta value is within its critical value. Therefore, in this design study, we employ principally NbTi superconducting magnet. We will consider Nb_3Sn as an alternative, when stronger

magnetic field becomes crucially necessary in future due to the fact that trapped particle instabilities are clarified to dominate the energy loss in higher temperature plasmas.

Setting B_{max} of 8 tesla and using Eqs. 4.5 ∿ 4.10, we determine the plasma and device parameters which enable us to attain the self-ignited state, as tabulated in Case I in Table 4.1.

4.3.5 Design by trapped ion mode scaling law

We now examine what plasma performances will be attained, if trapped particle instabilities are dominant in Case I. Figure 4.3 shows the attainable plasma performance of Case I estimated by using Eqs. 4.3 and 4.4. The region encircled by the frame in the figure is the target region. In the estimation, we have used the following values for numerical coefficients c_{TI} and c_{TE}.[5)]

$$c_{TI} = 1.93 \times 10^{37} \quad , \tag{4.11}$$

$$c_{TE} = 5 \times 10^{18} \quad . \tag{4.12}$$

These values have been obtained by assuming that $\frac{1}{n}\frac{\partial n}{\partial r} \sim \frac{1}{T}\frac{\partial T}{\partial r} \sim \frac{1}{a}$ (see Appendix Chap. 2). They may rather overestimate $\bar{n}\,\tau_E$ value and correspond to those of the so-called one-tenth trapped particle mode scalings.[9)]

If the trapped particle instabilities are excited and the energy loss is determined mainly by these instabilities and, moreover, if numerical coefficients c_{TI} and c_{TE} are smaller than those of Eqs. 4.11 and 4.12 by a factor of two or three, it is difficult to attain a self-ignited state in Case I. As shown in Eq. 4.3, τ_E can be highly improved by strengthening B_t. Thus, we can attain a self-ignited state, even when c_{TI} becomes one-third of Eq. 4.11, by replacing B_t coils with Nb_3Sn coils. This is shown in Table 1 as Case II. In Case II, if we take the same β_p value as that of Case I, the plasma density is excessively high ($\bar{n} = 3.6\times10^{20}$ m^{-3}). Therefore, the plasma beta value must be lowered than that of Case I to avoid excessively large fusion power and the surface heating of the plasma as will be discussed later. Figure 4.4 shows the attainable plasma performance of Case II estimated by using each scaling law.

4.4 Additional Heating

Up to this time, the most reliable method for the additional heating is the neutral beam injection (NBI) using positive ions. The effect of this method has already been proved in various experiments.[6)10)11)]

The RF heating method has a possibility to increase input heating power density up to about 10 kW/cm^2.[12)] When this is realized, this method will considerably reduce the difficulties in and the restrictions on the machine design. Although RF heating seems to be quite attractive, the effect of heating has not yet been made clear sufficiently. Thus, in this design study, we adopt only NBI heating using positive ions to obtain a required heating power. The injection energy and power are shown in Table 4.1.

4.4.1 Injection particle

We consider deuterium injection only. It is because injection of tritium will make the injector quite complicated. Since only deuterium is injected, tritium must also be supplied by puffing, pellet injection or some other ways to keep the fuel particle ratio always to be unity. Under this circumstance, some measure will be required to maintain the similar spatial distributions for deuterium and tritium particles.

4.4.2 Required injection power

It should be reasonable that about the same amount of the additional heating power as the α-particle heating power is sufficient for the plasma to be ignited. In fact, calculations by one dimensional simulation code with fixed distribution show that additional heating power of the order of α-particle heating can ignite the plasma, if the impurity concentration can be suppressed within a permissible level (Fig. 4.5, Fig. 4.6 and also Ref. (7)). Thus, we determine the required injection power to be nearly equal or slightly lower than the α-particle one.

4.4.3 Injection energy

We determine the injection energy from the condition that the plasma should be heated uniformly. Then, the required injection energy can be determined by[13)]

$$\bar{n}\, a^2 \lesssim \frac{c_h v_0}{\langle(\sigma_{cx} + \sigma_{ii} + \sigma_{ei})v_r\rangle} \quad , \tag{4.13}$$

where σ_{cx}, σ_{ii} and σ_{ei} are the cross section for charge exchange, impact ionization by ions and electrons, respectively. v_0 and v_r are the initial speed of the injected particles and relative speed between the injected particles and the background plasma particles, respectively. It is required that the numerical constant c_h be about 2 to avoid the surface heating.[13)]

In this design study, we set $c_h = 3.0$ on the ground that large α-particle heating can be expected in the center region in the latter period of NBI heating. This means that until the density reaches two-thirds of the target value, the plasma can be heated uniformly. After that, however, the plasma surface may somewhat be heated more than the plasma center by NBI heating. The curve (a) in Fig. 4.7 shows the required injection energy as a function of $\bar{n}$ a. As can be seen from this figure, the injection energy of at least 200 keV is required both for Case I and II, since the values $\bar{n}$ a are 2.2×10^{20} m^{-2} and 2.5×10^{20} m^{-2}, respectively.

4.4.4 Available injection power

As the injection energy becomes such a high energy, the neutralization efficiency will fall remarkably, so that it can become a serious problem whether or not the necessary injection power can be obtained. The curve (b) in Fig. 4.7 shows the available injection power calculated semi-empirically on the basis of design experience in JT-60, in which 20 MW heating power can be obtained by H^0 injection of 75 keV. According to this figure, $p_h \cdot a \sim 0.5$ MW/m^2 for 200 keV. Then, for the PETF plasma volume of 340 m^3, total injection power $p_h \cdot V$ of about 110 MW will be available. Thus, even when we take account of the structural restrictions by the shields and superconducting coils, the injection power of 50 $\sim$ 70 MW can reliably be obtained.

4.4.5 Relations to beta value

In Case II, the beta value is reduced to half that of Case I. If we set the beta value to be the same as in Case I, $\bar{n}\,\tau_E$ value can be increased by 4 times. In this case, however, $\bar{n}$ a value will become 4.5×10^{20} m^{-2}.

Consequently, NBI heating will become quite difficult. Thus, in this design study, avoiding the difficulties of NBI heating, we maximize $\bar{n}\ \tau_E$ value.

In case II, since $\bar{n}$ a cannot be increased more than that of case I by NBI limitation and since $n\tau \propto (\bar{n}\ a)^2$, $\bar{n}$ and consequently τ_E cannot be increased. Therefore, increased B_t will not give any advantage to the plasma confinement except for β which will be lowered sufficiently down from the β-limitation value.

In the case of trapped ion mode scaling, dependences of $\bar{n}\tau_E$ value on $\bar{n}$, a and B_t can be written as

$$(\bar{n}\tau_E)_{TI} \propto \bar{n}^2\ a^4\ B_t^2 = (\bar{n}\ a)^2\ a^2\ B_t^2\ , \tag{4.14}$$

from Eq. 4.3. Since a is fixed and $\bar{n}$ a value cannot be increased by the limit of NBI heating, the maximum $\bar{n}\tau_E$ value can be obtained by maximizing B_t. In other words; larger $\bar{n}\tau_E$ value can be obtained by reducing the beta value with raising B_t, rather than by raising the beta value with decreasing B_t.

4.5 Impurity Control

Plasma contamination by impurities will be one of the most serious problems in the future large tokamaks, since, even in the today's plasma, the energy losses due to impurities are most dominant and moreover, impurity productions will be enhanced in the large tokamaks by strong interactions of the plasma and the first wall because of higher temperature and longer duration time. Permissible impurity concentrations of carbon, oxygen and molybdenum for the self-ignition and related total radiation energy losses due to these impurity concentrations both of Case I and II are shown in Table 4.2. These permissible impurity concentrations are about an order of magnitude smaller than those in the present-day devices.

Impurity concentrations should be suppressed below their permissible levels by controlling their major production mechanisms such as evaporation and sputtering. At present, we adopt the following method as one of the most realistic and expectable candidate for impurity control:

A combination of the poloidal magnetic limiter whose limiter coils are installed outside the plasma chamber and the graphite wall and limiter plate with temperature control. In addition to this method, however, some

further measure of temperature control of plasma boundary region will be required to suppress the impurity concentrations below the permissible levels.

4.5.1 Permissible impurity concentration

In the present-day tokamaks, light impurities, such as carbon and oxygen partially ionized near the plasma boundary play a role of converting the energy flow carried by electron's anomalous transport into the radiation mostly due to excitation. As the plasma temperature rises in the future large tokamaks, even light impurities will result in center-cooling in the similar way as metallic ones, since the light ones will be ionized to a higher charge state because of their long confinement times. The excitation loss decreases and the bremsstrahlung loss increases especially in the central region of multi-keV.[14] Thus for light impurities, in the future higher temperature plasmas, the bremsstrahrung radiation loss will be dominant.

Heavy metallic impurities such as molybdenum are partially ionized even at the temperature above multi-keV and will cause radiation energy loss from the bulk plasma. Therefore, in the large tokamaks with high temperature, both light impurities and heavy metallic impurities cause radiation energy loss from the whole region of the plasma, so that the energy loss by impurities will be added to the energy loss by transport. Permissible impurity concentration can then be obtained from Eq. 4.6. For light impurities, the expressions for the bremsstrahlung radiation loss by Eq. 4.7 is used to obtain P_r, while for heavy impurities it is a difficult problem to estimate precisely the energy loss by them. There have been proposed many expressions for the energy loss by impurities.[14,16] Here, we use an approximate expression of these energy losses per unit volume, p_r, as

$$p_r = 10\left[\frac{\bar{n}_i}{10^{20}}\right]^2 \frac{N_z}{N_i} \times 10^2 \, M_z{}^3 \qquad (MW/m^3) \ , \tag{4.15}$$

where $\bar{n}_i$ and N_i are the mean ion density and the total number of ion, respectively, and M_z is the atomic mass number. This expression is derived from the results of calculating the density distributions of impurities and the related energy losses in a large tokamak, taking into account impurity diffusions and ionization processes.[14]

Permissible impurity concentration $f = N_Z/N_i$ and the related total energy losses by these impurity concentrations for carbon, oxygen and molybdenum, which are calculated by using Eqs. 4.6, 4.7 and 4.15, are shown in Table 4.2.

Considering the fact that, even in the present-day tokamaks, of which ion temperature is of the order of 1 keV, the plasmas are contaminated by light impurities of about several percents or by heavy metallic impurities of about 0.1%, it will be a quite severe requirement to supress the impurity concentrations below these permissible levels in the future large tokamaks, in which the interactions between plasmas and the first wall will inevitably be strengthened due to the higher plasma temperatures and longer duration times.

First of all, it is necessary to suppress the impurity production due to evaporation and sputtering from the first wall. According to Table 4.2, the limiter will suffer from a heat load of 30 $\sim$ 40 MW, if any control of the plasma edge temperature is not performed. In this case, evaporation of the limiter will become a serious problem. In addition, the increase of the energy of bombarding particles due to the higher edge temperature will increase the sputtering of the first wall materials.

Secondoly, shielding effect with fairly high efficiency will be required to prevent the inflow of the sputtered and evaporated first wall materials. At present, only a poloidal magnetic limiter seems to have a potentiality to meet the above requirements to a certain extent. Moreover, its realistic design will also be possible. We will discuss the poloidal magnetic limiter in the following section.

4.5.2 Magnetic limiter

There are three types of the magnetic limiter; the toroidal magnetic limiter, the bundle divertor and the poloidal magnetic limiter. Since the former two types of magnetic limiter will produce 100% ripple in toroidal magnetic field, the ripple diffusion will become a serious problem. Furthermore, it is a matter for question whether a realistic design of the magnetic limiter coil is possible or not, since the stress of the coil will become quite large. Thus, we examine the poloidal magnetic limiter, whether it can be designed realistically or not.

1) heat load

First, we estimate the heat load on the magnetic limiter plate. If we

install two magnetic limiters at upper and lower tops of the plasma, the heat load P_ℓ on the magnetic limiter plates will be

$$P_\ell = \frac{P_L}{4\times 2\pi R\delta} \sim 1 \quad kW/cm^2, \tag{4.16}$$

where P_L is the total energy loss from the plasma conveyed by plasma particles and is about 40 MW both in Case I and II. The δ is the width of the scrape-off layer plasma and is of the order of $2 \sim 3$ cm. This heat load is excessively large and evaporation of the limiter plates will become a serious problem. One possibility to solve this problem is to swing the magnetic lines of force intersecting the limiter plates. In fact, if we swing the lines of force to sweep the limiter plates over the area of which width is about five times larger than that of the scrape-off layer, the heat load of Eq. 4.16 will be reduced to about 200 W/cm^2. This method will significantly mitigate the restrictions on the design of cooling mechanism for the limiter plates, and evaporation can possibly be avoided. The experiment on the swing of the lines of force will be carried out in JT-60 and the effectiveness of this method is expected to be clarified.

It is questionable, however, that this method for reducing the heat load is applicable to future reactors. Since $P_\ell \propto a^{1/2}P_W$ (P_W: the wall loading, a : the plasma minor radius), P_ℓ is expected to be increased by several factors, so that the lines of force will have to be swung in proportion to this increase of P_ℓ. A realistic design of such a large swing will become quite difficult. For PyG as low Z materials, because of its high thermal conductivity along the deposition plane, there is a possibility to withstand the heat load of Eq. 4.16 even without swinging the lines of force, if the reliable cooling mechanism of the limiter plates is developed. Furthermore, if the edge temperature is severely controlled in order to suppress the impurity production due to sputtering, the heat load of the limiter plates will significantly be mitigated. It is because, in these systems, the dominant part of the energy flow by the transport is converted into radiation or charge exchange energy flow. In such systems, too, the limiter plates may withstand the heat load without swinging the lines of force.

2) shielding effect

Another important role of the magnetic limiter is a shielding effect, which prevents the influx of sputtered and evaporated first wall materials.

As will be shown in the following section, in addition to some edge temperature control, shielding effect of more than 80 ∿ 90% will be required even when only impurity production by sputtering is taken into account. The experiments by the present-day tokamaks, for example, DIVA, have proved that the scrape-off layer plasma has a shielding effect of about 90%.[17] In the next generation machine as PETF, the value of $n_s\delta$ (n_s: mean plasma density of scrape-off layer) is likely to decrease as $1/\sqrt{T_a}$ (T_a: edge temperature of the plasma) in comparison with that of DIVA. When the edge temperature control is severely performed, T_a will not differ so much from that of the present-day plasma. In this case, the shielding effect of about 90% can be expected in PETF.

3) relations to remote handling

From the view point of the remote assembly and maintenance, the poloidal magnetic limiter will cause a serious difficulty. Especially, when the limiter coil is installed inside the vacuum vessel, the ingeneous remote handling will be required. Thus, the contrivance to install the limiter coils outside the vacuum vessel maintaining the null points inside the vacuum vessel, is indispensable. Although considerable difficulty is anticipated to install the limiter coils including sub coils which might be necessary for the plasma stability outside the vacuum vessel, there seems to be no solution except this contrivance from the view point of the remote handling.

In this case, the magnetic limiter coils will be buried in the shields so that we can expect that neutron radiation damage of the coils will be somewhat mitigated than in the case of the inside coils.

4.5.3 Choice of materials for the first wall

As the first wall materials, there are two major candidates; low Z materials such as graphite and high Z materials such as molybdenum. The materials should be determined in terms of the potential to meet the requirement for impurity control. As was discussed in the preceding section, there is enough prospect of avoiding the evaporation by using the poloidal magnetic limiter and swinging lines of force. Thus, in this section, we discuss which material is more advantageous for sputtering.

We consider the sputterings of the first wall materials by plasma ions, and by fast charge exchange neutrals. We also take account of the self-

sputtering by impurity ions. Each sputtering yield is denoted by R^+, R^0 and R_s, respectively. R^+ and R^0 include the chemical sputtering. Impurity ions sputtered are assumed to be shielded by the scrape-off layer plasma of temperature T_a with shielding efficiency ζ. Under this situation, impurity concentration $f = N_z/N_i$ in steady state is given as[18] (see Ref. (23) in detail)

$$f \equiv \frac{N_z}{N_i} = (1 - \zeta) \frac{R^+ + \frac{\gamma}{1-\gamma} R^0}{1 - R_s(1 - \zeta)} \frac{\tau_z}{\tau_n} \quad , \tag{4.17}$$

where τ_n and τ_z are the confinement times for the plasma ions and impurities, respectively. γ is the escaping ratio of charge exchange neutrals to the total inflow of recycling particles. R^+, R^0 and R_s are determined by T_a. According to the experimental results of DIVA, the scaling for T_a is given, for the PETF's design value, as

$$T_a \sim 2.8(1 - \tilde{p}) \qquad \text{(keV)} \quad , \tag{4.18}$$

where

$$\tilde{p} = \frac{P_{cx} + P_r}{P_{in}} \quad . \tag{4.19}$$

where P_{in}, P_{cx} and P_r are the input power to the plasma, energy loss powers due to charge-exchange and radiation, respectively. $\tilde{p}$ is the ratio of the energy loss powers due to charge exchange and radiation to the input power. This value represents a measure of the edge temperature control.

1) Low Z materials

It has been proposed and investigated that low Z materials such as carbon and carbide may be advantageous for the first wall materials, since their permissible levels of contamination in the plasma are by two orders of magnitude larger than metallic ones. However, their advantages are not yet decisive, since their sputtering yield by chemical reaction are by nearly two orders of magnitude larger than those of metallic ones in the temperature range of the first wall of 400 ∿ 800°C. The sputtering yield by chemical reaction is not so large in the temperature range of below 300°C and around about 1000°C. Therefore, we must control the first wall temperature in the advantageous ranges mentioned above, if we expect the advantages of low Z materials. We now discuss the advantage and disadvantage of the low Z materials quantitatively.

In the case with small chemical sputtering, $\zeta \gtrsim 70\%$ is sufficient to suppress the impurity concentration below 1%, even when $\tilde{p}$ is 0.5. This requirement can be met relatively easily. Furthermore, in this case, lower $\tilde{p}$ is preferable to lower the required ζ. Thus, if we can avoid evaporation, blistering and erosion of the first wall, and if we can control the first wall temperature in the advantage region (below 300°C or around about 1000°C), carbon first wall will be able to satisfy the requirement for the impurity control quite satisfactorily.

In the case with large chemical sputtering, $\zeta \gtrsim 95\%$ will be required regardless of $\tilde{p}$. This requirement for ζ seems to be quite difficult. Thus, chemical sputtering must be suppressed by all means.

2) High Z material

We evaluate the required ζ and $\tilde{p}$ for the molybdenum first wall. Equations 4.17 ∿ 4.19 can also be used. $\tilde{p} \gtrsim 0.97$ will be required to suppress the impurity concentration below 0.01% even when $\zeta \gtrsim 90\%$ is realized. It seems to be quite difficult to meet this requirement even when various measures are taken. The situation $\tilde{p} = 0.97$ means that 97% of the energy loss carried by plasma particles must be converted into the charge exchange and radiation loss in the periphery.

There have been proposed several methods to meet this requirement for the edge temperature control. Among them are 1) energy conversion into radiation by suitable light impurities in the periphery[20], 2) energy conversion into charge-exchange loss in the periphery (gas insulation)[21]. Both of them have not yet been proved.

Another method to mitigate the above requirements has been proposed, that is, the reduction of the sputtering yield by honey-comb structure.[22] This structure can reduce by 1/20 the effective sputtering yield of heavy incident particles. Although the effect of light incident particles has not yet been made clear, we can expect 1/3 reduction at least. When we take 1/20 reduction, $\zeta \gtrsim 92\%$ is sufficient to suppress the impurity concentration below 0.01%, when $\tilde{p} = 0.9$ is realized. This may be realizable somehow by various measures. If we take 1/3 reduction, $\zeta \gtrsim 99\%$ is still required when $\tilde{p} = 0.9$ is realized. This requirement is still quite difficult.

In conclusion, we evaluate, at present, that the low Z materials are more advantageous than the metallic ones. The latters are taken as an

alternative. Final decision will be made after we realize a reliable design of first wall temperature control for low Z materials, and prove a reduction effect of honey-comb liner on light incident particles for metallic ones.

4.6 Ash Exhaust

In this design study, we do not install any particular mechanism for helium ash exhaust. The reasons for this determination are as follows.

1) The accumulation of helium ashes will reach at most up to about 10% for 30 sec burn time and about 20% for 60 sec burn time unless they are exhausted. These amounts of ash accumulation may not deteriorate the plasma performance so much, except that the plasma beta value is slightly increased to keep the fuel amount constant.

2) Moreover, it is difficult to attain high exhaust efficiency due to the technological restrictions as follows. It is not acceptable to install the pumping mechanisms inside the toroidal field coils, since in this case extremely large coils are required. Hence, the major part of pumping mechanisms should be installed outside the coils, i.e. volume pumping. However, simple pumping around the plasma periphery is not an adequate method, since the coils and structure limit the gas pumping conductance (we can expect exhausting port area only a few percent of the total wall surface area) to a level at which equilibrium can be achieved only at high ash pressure at the periphery. Even in the case with a poloidal magnetic limiter which pulls plasma particles from the edge region into a second chamber, we can expect an exhaust efficiency of only about 10%.

Thus, no appreciable ashes can be exhausted during the burn phase of PETF.

(M. Sugihara)

References

1) E. Apgar, et al.: Proc. 6th Int. Conf. Plasma Physics and Controlled Nuclear Fusion Research, Berchtesgaden, (1976) 1, IAEA, Vienna (1977) 247.
2) C. Daughney: Nuclear Fusion 15 (1975) 967.
3) J. Hugill and J. Sheffield: Nuclear Fusion 18 (1977) 15.
4) B.B. Kadomtsev and O.P. Pogutse: Nuclear Fusion 11 (1971) 67.

5) S.O. Dean et al.: WASH-1295 (1974).

6) H. Eubank, et al.: 7th Int. Conf. Plasma Physics and Controlled Nuclear Fusion Research, Innsbruck, 1978, IAEA-CN-37-C-3.

7) M. Sugihara, M. Kasai, T. Tazima and T. Hiraoka: JAERI-M 7885 (1978).

8) Y.K. Peng, R.A. Dory, B.B. Nelson and R.O. Sayer: Phys. of Fluids 21 (1978) 467.

9) T. Ohkawa: GA-A14273 (1977),
J. Clarke: ORNL/TM-5860 (1977).

10) L.A. Berry, et al.: Proc. 6th Int. Conf. Plasma Physics and Controlled Nuclear Fusion Research, Berchtesgaden, (1976) 1, IAEA, Vienna (1977) 49.

11) Equipe T.F.R.: ibid. 35.

12) T. Nagashima: Private communication.

13) S. Matsuda and H. Yamato: JAERI-M 6222 (1975).

14) T. Tazima, Y. Nakamura and K. Knoue: Nuclear Fusion 17 (1977) 3.

15) D.M. Meade: Nuclear Fusion 14 (1974) 289.

16) R.V. Jensen, D.E. Post, W.H. Grasberger, C.B. Tarter and W.A. Lokke: Nuclear Fusion 17 (1977) 1187.

17) M. Nagami, et al.: Nuclear Fusion 18 (1978) 1347.

18) T. Tazima: JAERI-M 7717 (1978).

19) DIVA Group: JAERI-M 7610 (1978).

20) Y. Shimomura: Nuclear Fusion 17 (1977) 626.

21) B. Lehnert: Nuclear Instruments and Methods 129 (1975) 31.

22) T. Abe, et al.: J. Nuc. Sci. Technol. 15 (1978) 471.

23) T. Tazima and M. Sugihara: to be published in JAERI-M (1979).

Table 4.1 Summary of plasma and device parameters of PETF

1)	Device parameters		
	Major radius (R)	6.2 m	
	Minor radius (a)	1.4 m	
	Ellipticity (K)	1.5	
	Triangularity (δ_t)	0.5	
	Aspect ratio (A = R/a)	4.43	
	Distance between the inside surface of plasma and the straight part of the inner perimeter of D-shaped toroidal field coil (Δ)	1.1 m	
	Safety factor (q_a)	2.5	
2)	Plasma parameters	Case I	Case II
	Toroidal coil	NbTi	Nb_3Sn
	Maximum field (B_{max})	8 T	12 T
	Field at plasma center (B_t)	4.8 T	7.2 T
	Plasma current (I_p)	4.9 MA	7.4 MA
	Average temperature ($\bar{T}$)	7 keV	7 keV
	Average density ($\bar{n}$)	1.6×10^{20} m^{-3}	1.8×10^{20} m^{-3}
	Beta poloidal (β_p)	3.0	1.5
	Beta toroidal (β_t)	4.0 %	2.0 %
	Confinement time (τ_E)	5.6 sec	6.4 sec
	Impurity concentration (Molybdenum)	6×10^{-3} %	9×10^{-3} %
	Total power (P_{total})	260 MW	340 MW
	Neutron wall loading (P_n)	0.5 MW/m^2	0.6 MW/m^2
	NBI heating power (P_{inj})	50 MW	70 MW
	NBI injection energy (E_b)	200 keV	200 keV
	Burn time	30∿60 sec	30∿60 sec
	Pulse interval	20 min.	20 min.

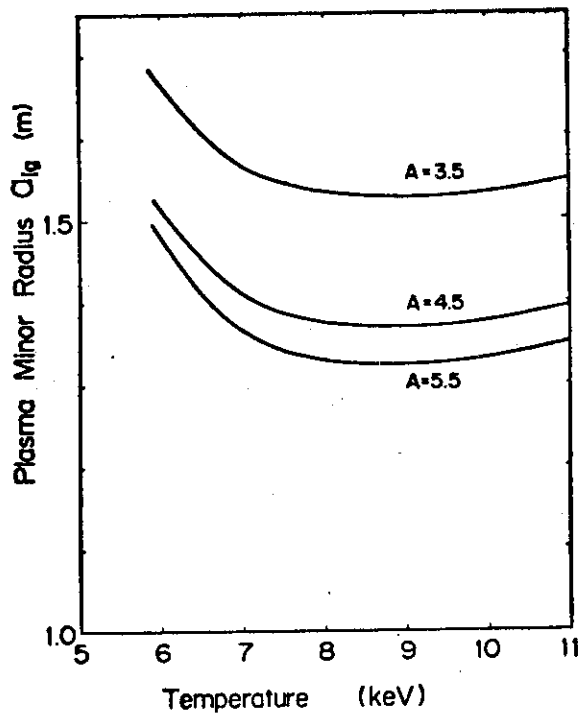

Fig. 4.1 Temperature dependence of plasma minor radius required for the self-ignition. $\bar{n}a^2$ scaling law is employed. B_{max} = 8T, Δ = 1.1m, β_p = 2/3A, K = 1.5, q_a = 2.5, Z_{eff} = 1.3

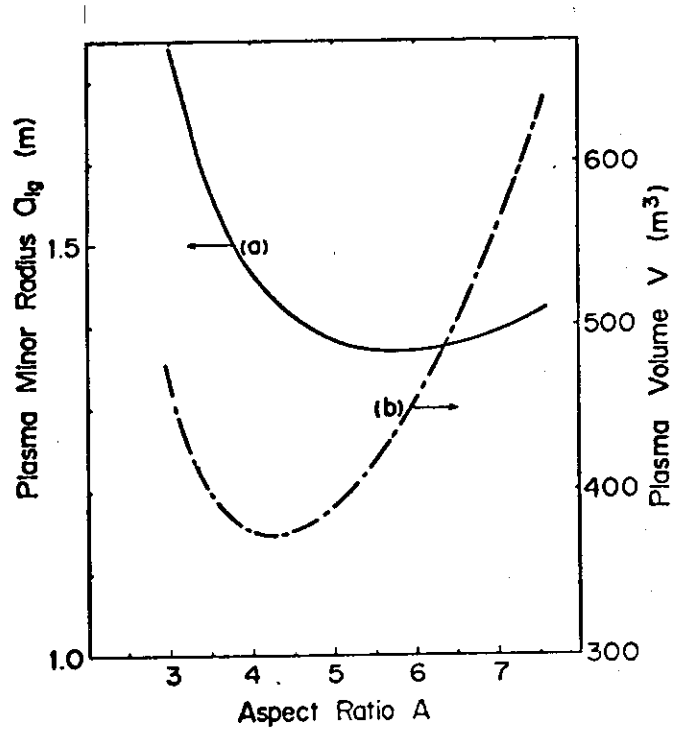

Fig. 4.2 Aspect ratio dependence of plasma minor radius and plasma volume required for the self-ignition. $\bar{n}a^2$ scaling law is employed. $\bar{T}$ = 7keV, B_{max} = 8T, Δ = 1.1m, β_p = 2/3A, K = 1.5, q_a = 2.5, Z_{eff} = 1.3.

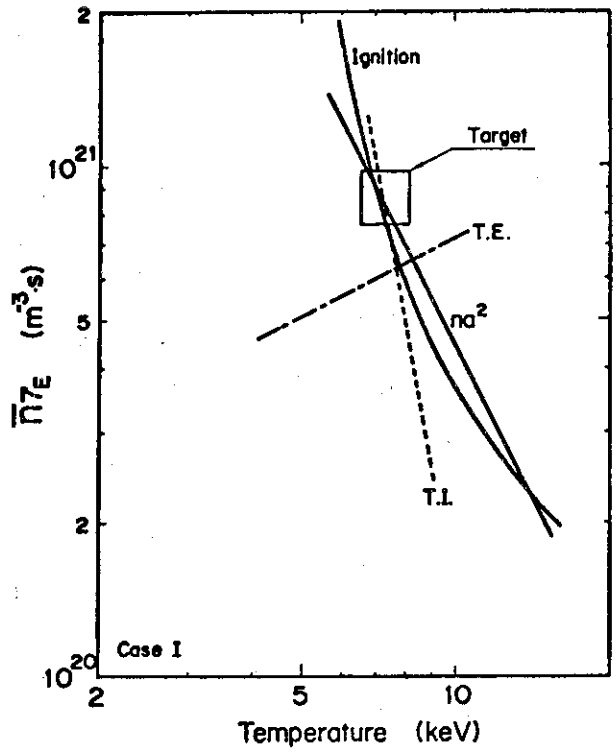

Fig. 4.3 Attainable plasma performance of Case I estimated by various scaling laws. B_{max} = 8T, $\bar{n}$ = 1.6×10^{20} m^{-3}.

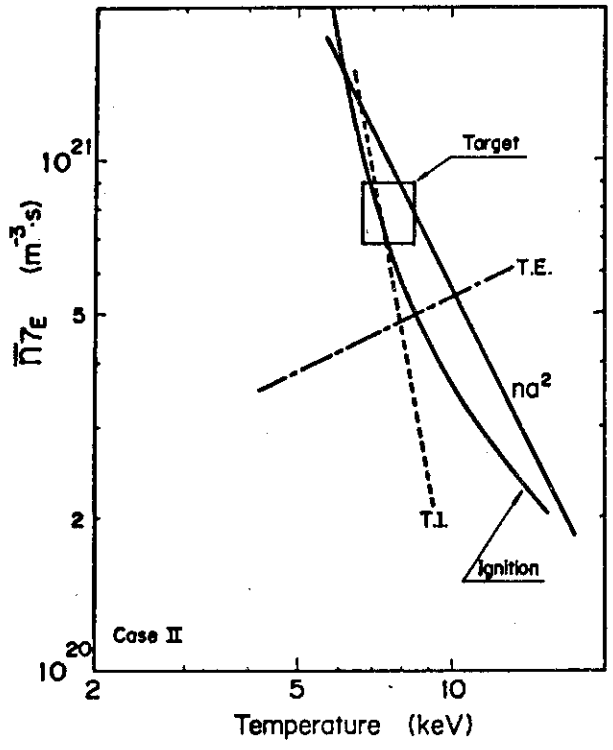

Fig. 4.4 Attainable plasma performance of Case II estimated by various scaling laws. B_{max} = 8T, $\bar{n}$ = 1.6×10^{20} m^{-3}.

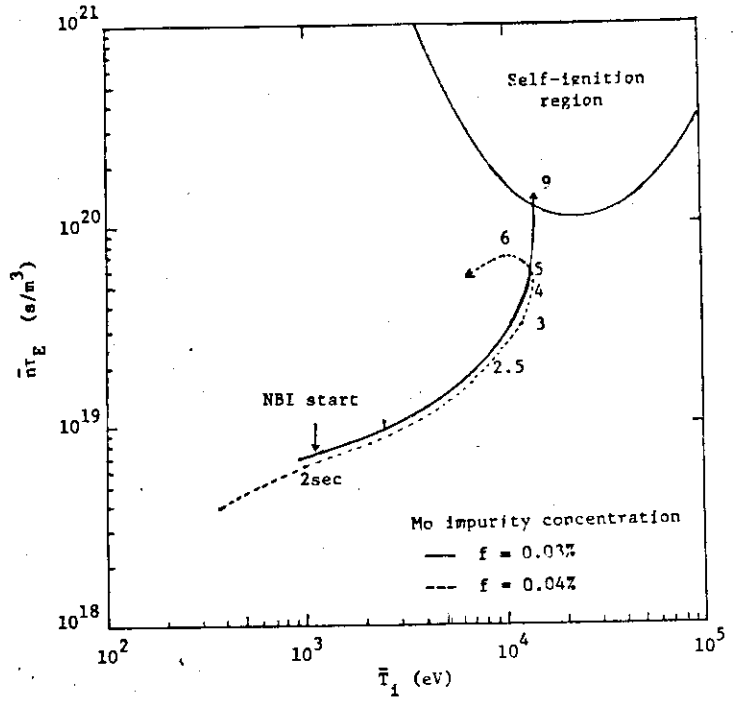

Fig. 4.5 Ignition approach of PETF in the case of $\bar{n}a^2$ scaling law. One-dimensional simulation code with fixed distributions of temperature and density is used. Injection heating power of 50 MW is started at t = 2 sec.

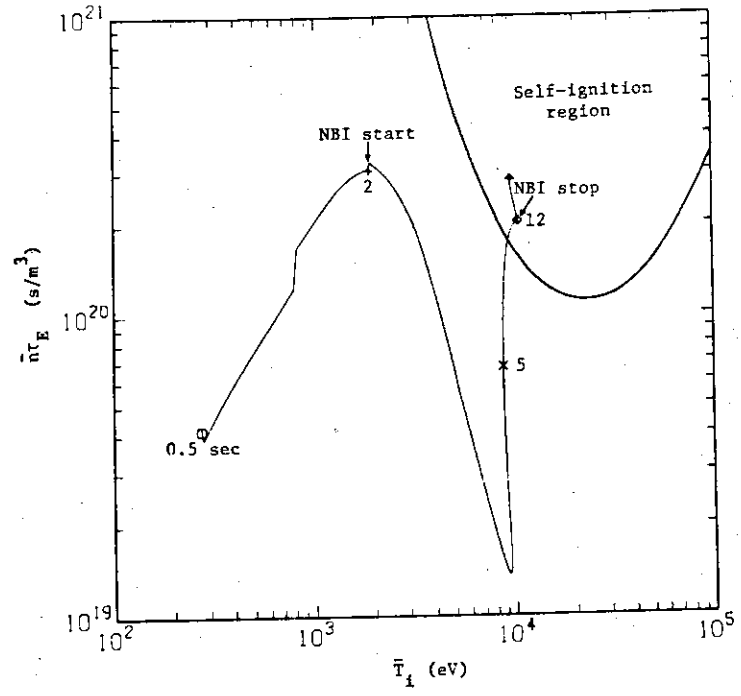

Fig. 4.6 Ignition approach of PETF in the case of one-tenth trapped particle mode scaling laws. One-dimensional simulation code with fixed distributions of temperature and density is used. Injection heating power of 50 MW is started at t = 2 sec.

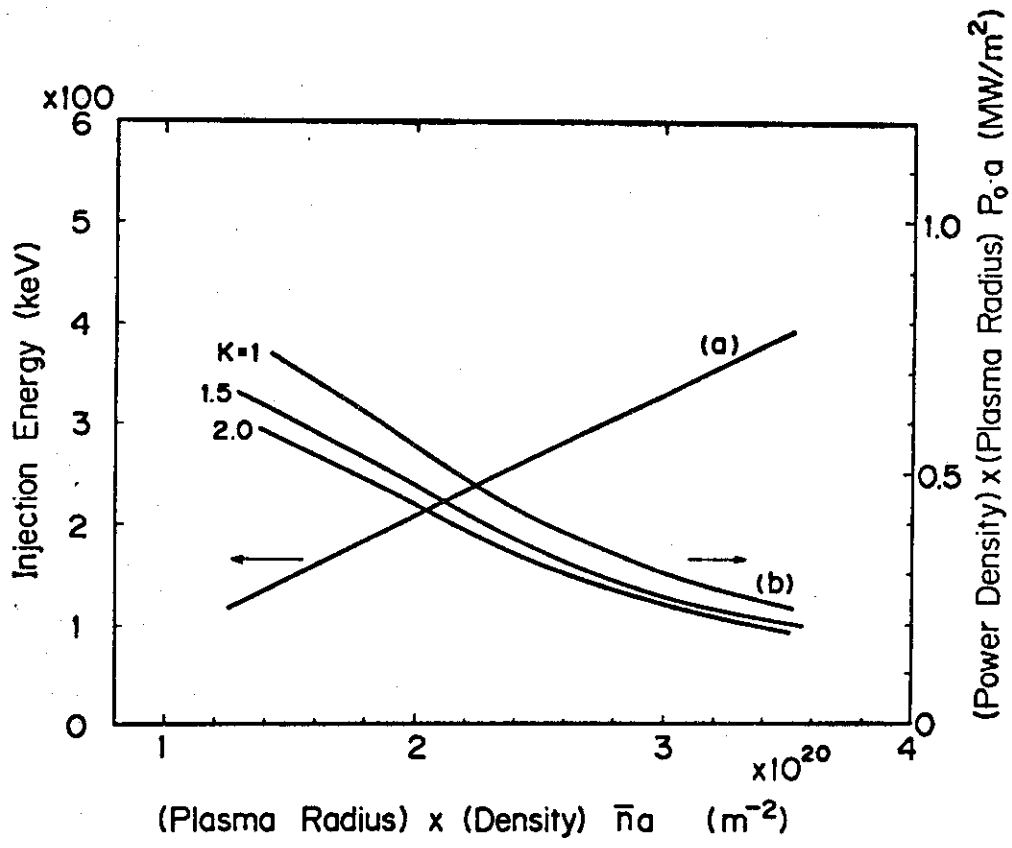

Fig. 4.7 Required injection energy and available injection heating power vs. $\bar{n}a$.

Table 4.2 Permissible impurity concentration of C, O and Mo and related energy losses in Case I and II

Impurity \ Case	Case I	Case II
C	f = 0.56 % Z_{eff} = 1.2	f = 1.3 % Z_{eff} = 1.5
O	f = 0.37 % Z_{eff} = 1.2	f = 0.84 % eff = 1.5
Mo	f = 6.4×10^{-3}% Z_{eff} = 1.1	f = 9.0×10^{-3}% Z_{eff} = 1.1
P_{loss}	14 MW	21 MW

5. Tokamak Machine

5.1 Plasma Chamber

5.1.1 Design considerations

At design of the plasma chamber of PETF, the following particular items should be taken into account for determination of the fundamental structure.

- One-turn electric resistance
- Electromagnetically induced force
- Remote handling
- Heat load to the limiter

1) One-turn electric resistance

Considerable one-turn electric resistance is required for the plasma break down. If this requirement is above 0.5 mΩ, bellows structure is inevitable. However, the bellows structure is not desirable to bear the various kinds of strong force, especially the electromagnetically induced force at plasma dump. If the resistance much lower than 0.5 mΩ is sufficient, we can employ the simple structure without bellows, i.e. the torus tube structure. In this case, the double-walled structure can be designed without excessive complication. This structure can provide a cooling and baking channel of the chamber between the walls. In addition, a fluid flow can serve the carrier of tritium leaking through the inner wall.

2) Remote handling

As explained in the section 4.4, we cannot help to employ the poloidal magnetic limiter to aboid evaporation of the limiter surface material and shield the influx of sputtered impurities. However, the magnetic limiter will make remote handling at assembly and disassembly extremely difficult. We can reduce considerably this difficulty if it is installed outside the vacuum vessel.

3) Heat load to the magnetic limiter plate

Even in the case of the magnetic limiter installed at the upper and lower tops of the vessel, the magnetic limiter plates will suffer a heat load of about 1 kW/cm^2. When we employ the limiter plates made of metal with high heat conductivity such as Mo with cooling mechanisms, we have to reduce evaporation by swinging the separatrix line.

On the other hand, low Z materials may be preferable for the liner plates from physical considerations. However, there will arise technological difficulty as follows. In general, poor heat conductivity of low Z material will cause the more intense evaporation. Possible candidate is pyloritic graphite (P_yG), which has considerably high heat conductivity along the deposition plane. Some reliable idea in design is required to make the most of this heterogeneity.

5.1.2 General description

The PETF's plasma chamber consists of the vacuum vessel, the poloidal magnetic limiter, the low Z liner if necessary, and the toroidal material limiter.

The vacuum vessel has the double-walled structure of stainless steel cooled by helium gas and has one-turn electric resistance of 0.5 mΩ. It can be also baked up by flowing hot helium gas. It is supported by the primary shield at its inner, outer, top and bottom positions to make the thermal displacement of its center minimum, as shown in Fig. 2.1. The supports have sliding mechanism to release the tangential thermal expansion.

The front surface (plasma side) of the chamber will be covered by low Z liner such as carbon because of the plasma impurity control.

The magnetic limiter plates are made of low Z material from the same reason as liner. The magnetic limiter coils are installed outside the vessel for easy assembly and disassembly.

The chamber has 16 sectors divided by 16 toroidal field coils. Two of them serve for the blanket test zone, eight for NBI ports, two for the vacuum ports and four for plasma diagnostics.

The neutron wall loading is about 0.5 MW/m^2, and the maximum neutron flux is about $3 \times 10^{14}/cm^2 \cdot sec$ at the first wall.

5.1.3 Vacuum vessel

In the followings, the main items affecting the design of the PETF's vacuum vessel are discussed.

1) Material

Candidate materials for the vacuum vessel are stainless steels (such as 316SS), nickel base alloys (such as Inconel 625) and titatium based alloys (such as Ti-6Al-4V). Among these three sorts of material, the

stainless steel is employed at present in the concept studies of the vessel because of its popularity with the accumulated data under irradiation.

2) One-turn electric resistance

Most of the present-day tokamaks use bellows in the vacuum vessel to satisfy the required one-turn electric resistance. The bellow structure is not desirable to bear the various kinds of strong force, especially the electromagnetically induced force at plasma disruption.

The vessel shown in Fig. 5.1.1 has one-turn electric resistance of 0.5 mΩ. This structure has sufficient strength without bellows although it is complicated a little bit. The lower one-turn electric resistance required for the plasma break down and the plasma current rise may be expectable in larger tokamaks. In fact, the break down and the current rise of the plasma was successful in Doublet III with resistance of about 0.2 mΩ which is much lower than those of today's tokamaks. The simplier chamber than that in Fig. 5.1.1 can be designed with Inconel 625, if the required resistance is lower than 0.2 mΩ.

Development of a reliable dielectric flange can offer the complete solution to the requirement for one-turn electric resistance.

3) Tritium leakage

Some amount of tritium will permeate the inner wall of the vacuum vessel, while the tritium leakage to the environment must be suppressed below the permissible level. Hence the vessel wall should have a double-walled structure which can provide the channel with sweep gas flow. Helium is very favorable gas for tritium sweeping. Cool helium gas can also serve as the wall coolant. Moreover, hot helium gas can bake the vessel to attain a high vacuum, and to desorb tritium from the wall before repairing PETF.

4) Electromagnetically induced forces

The operating temperature of the stainless steel vessel should not exceed 500°C because of their mechanical properties. Neutron heating rate at the PETF vessel will be 7 W/cm^3 at most. This heat load is low enough to keep the vessel temperature below 300°C.

The rough estimation shows that the vacuum vessel will suffer the impulsive pressure loads of the order of ±10 kg/cm^2, which are most stringent, due to the eddy currents induced at plasma diminishing in 5 msec. Since the vessel shown in Fig. 5.1.1 is composed of I beams and pipes, the

induced eddy currents will be relatively small. Moreover, pipes inserted between I beams can absorb the thermal expansion of the vessel.

5.1.4 Magnetic limiter

Since it is very essential to keep impurity concentration at the quite low level in PETF as described in the section 4.4, we cannot help to employ the poloidal magnetic limiter installed outside of the upper and the lower tops of the vacuum vessel as shown in Fig. 5.1.2.

In the followings, main items affecting the design of the magnetic limiter are discussed.

1) Magnetic limiter coils

The magnetic limiter coils installed inside the vessel will make the assembly and disassembly extremely difficult. On the other hand, if we can install them outside the vessel, the working space and the personal accessibility to the magnetic limiter coils can be remarkably improved.

We found the solution to make null points inside the vessel with the coils installed outside the vessel as shown in Fig. 5.1.2.

2) Magnetic limiter plates

Even when we employ the poloidal magnetic limiter installed at the upper and the lower tops of the vessel, the magnetic limiter plates will suffer a large heat load.

As mentioned in the section 4.4, the energy loss to the limiter carried by plasma particles is 30 $\sim$ 40 MW during burning phase of 30 $\sim$ 60 seconds. The width of the scrape off layer will be 2 $\sim$ 3 cm. Therefore, the heat flux to the limiter plates is about 1 kW/cm^2.

The plate thickness should be probably more than 0.5 cm to withstand the run away electron bombardment. On the other hand, in the case without swinging the separatrix, the preliminary analysis of thermal stress under normal operating condition requires the plates made of high thermal conductive metal with thickness of about 0.1 cm and to be cooled by high velocity ($\sim$10 m/sec) flow of water.

Low Z materials may be preferable for the liner plates from the viewpoint of the impurity control as mentioned in the section 4.4, although it has some mechanical difficulties. In general, it is more difficult for the low Z limiter than for the metallic limiter plates to avoid evaporation because of its poor heat conductivity. The exceptional one is PyG, which

has fairly high heat conductivity along the deposition plane. Moreover, PyG is advantageous for thermal stress because of high thermal conductivity along the dpoisition plane, small Young's modulus and small thermal expansion coefficient.

A reliable design of PyG limiter plates with cooling mechanism is one of the essential items for R & D.

5.1.5 Liners

When we employ the vessel structure of the thick tube torus, liner to cover the vessel wall will be unnecessary except for the local one to protect the runaway electrons at plasma dump and the injected neutral beam penetrating the plasma.

If the vessel is made of unfavorable material for impurity control, its surface should be covered by the liner made of favorable one. However, when we can develop a reliable clad-metal consisted of the vessel material and favorable one, or develop a reliable method of plating preferable materials on the vessel to sufficient thickness, the liner plates will be unnecessary. The difference of their thermal expansion coefficients in the clad-metal or the exforiation in plating will prevent their realization.

The technological problems about the liner are discussed in the following.

1) Electromagnetically induced force

The liner will suffer extremely strong electromagnetically induced force due to the eddy currents at the plasma dump. To reduce this force, we must devide the liner into many small pieces of plates whether it is made of metals or low Z materials. However, the design of their reliable support structure is quite difficult.

2) Heat load

As mentioned in the section 4.4, the liner will suffer the continuous heat loads of 7 W/cm^3 neutron heating and of 5 W/cm^2 radiation heat flux from the plasma. The saturated temperature of the liner plates after successive shots will go up to about 700°C with low Z material, and 1000°C with Mo. The temperatures will be stringent for Mo plates because of low yield strength but not so much for PyG.

However, this temperature is not desirable for PyG from the viewpoint of impurity control. Low Z material, especially carbon, is considered as

preferable one for the first wall material because of its higher permissible level of contamination in the plasma than that of metal by two orders of magnitude. However, this advantage will be canceled, since its sputtering yield by chemical reaction is by nearly two orders of magnitude larger than those of metallic ones in the temperature range of 400 ∿ 800°C. Therefore, when we employ carbon for the liner material, we should control the liner temperature below 300°C or at about 1000°C to suppress this chemical sputtering yield. However, it is difficult to meet above requirement, unless we can find a reliable design of a support structure of the low Z material liner, by which the heat load can be sufficiently transfered from the liner to the chamber.

From above considerations, we temporalily employ the low Z material liner. We leave the final decision after further design studies and R & D.

5.1.6 Material limiter

The plasma of PETF should be well apart from the wall surface by controlling its equilibrium position and separatricies with the poloidal magnetic fields. However, when we are failed to control them or there occur the plasma disruption, the plasma contacts with the wall and large heat load deposits locally on the wall. It will cause damage of the liner and consequently of the vessel wall.

Therefore, it is preferable to install the material limiter on the liner against these plasma bombardments. By this way, we can more readily repair the material limiter than the liner by remote handling because they are located at the definite positions.

(M. Kasai)

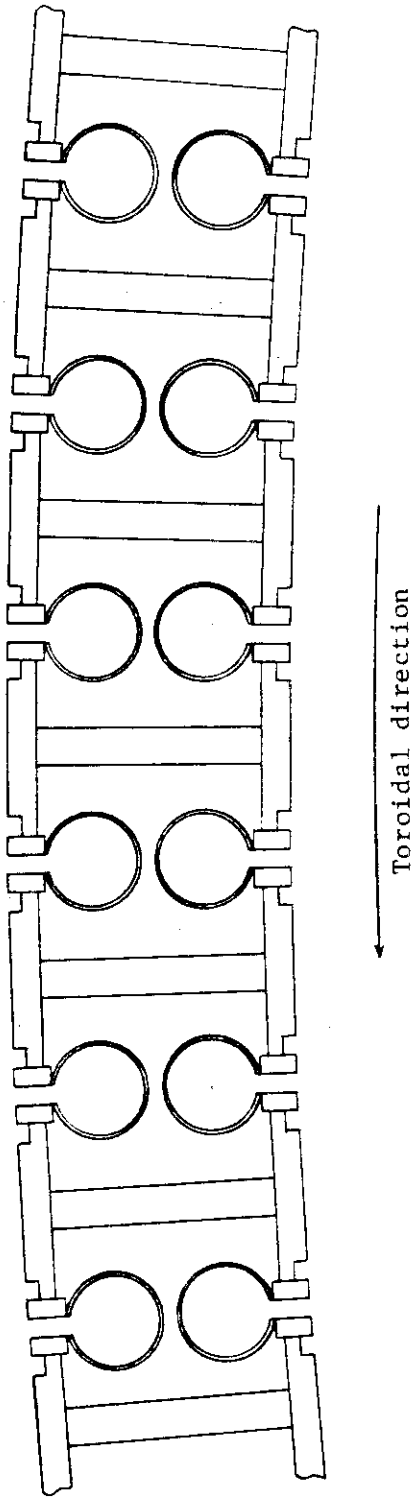

Fig. 5.1.1. Crosssectional view of vacuum vessel

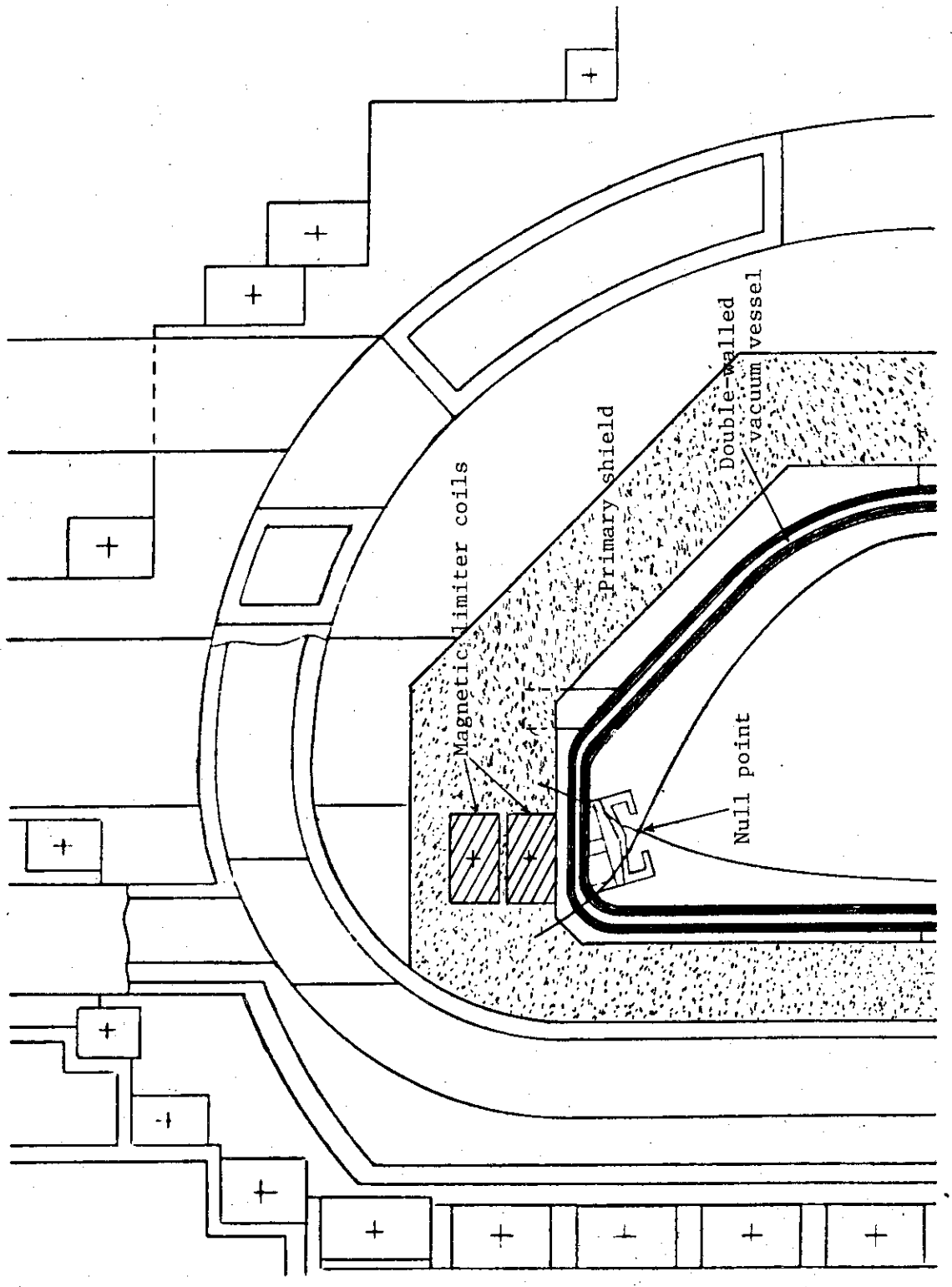

Fig. 5.1.2 Arrangement of magnetic limiter coils

5.2 Radiation Shield

5.2.1 General description

Two kinds of radiation shield surround main body of PETF to attenuate neutron and gamma ray flux. One of them is the primary shield for toroidal field coils and the secondary one is the biological shield. The primary shield is installed between the vacuum vessel and the toroidal field coils. It stands on its own legs, and supports the vacuum vessel at four positions. It consists of the stainless steel layers cooled by borated water, the heavy concrete and lead if necessary. Its thickness is 60 cm in the inner part and 90 cm in the outer, upper and lower parts.

The secondary shield supplements the primary one for biological shield with the wall of the reactor building. It is made of concrete brocks, and supported by the framework of PETF. The 1.5 m thick concrete brocks installed above PETF can decrease the sky shine and reduce the ceiling thickness.

5.2.2 Primary shield

The toroidal field strength at the plasma axis B_{to} is very sensitive to the distance between the inside surface of plasma and the straight part of the inner perimeter of D-shape toroidal field coils. Therefore, with the fixed maximum toroidal field strength at B_t coils, it is very important to reduce the thickness of the shield layer as thin as possible from the viewpoint of plasma engineering.

On the other hand, the minimum thickness of the inner shield should satisfy the following requirements.

a) The shield layer should be thick enough to reduce the heating rate by radiation less than the permissible level in the superconducting toroidal field coils.

b) The shield layer should be thick enough to reduce the radiation damage rate less than the permissible level in the superconducting toroidal field coils.

The thickness required for the item a) is evaluated to be thicker than that of item b) in PETF because of the small duty factor of about 0.05.

The 60 cm thick shield is required to suppress the heatiang rate in the toroidal field coils under 10^{-3} W/cm^3 which raises the coil temperature about 1 degree.

In determing the thickness of the outer region, the personal accessibility to the tokamak equipment should be also considered as well as items a) and b) for easy attachment of automatic remote handling equipments or for adjustment work of plasma diagnostic systems. The thickness more than 90 cm is required to enable persons to access to the outside of the tokamak after 24 hours from the shut down.

5.2.3 Secondary shield

The wall of the tokamak building will serve as biological shield. The one dimensional spherical calculations with the spherical neutron and γ ray sources indicate that the 2 m thick concrete wall can attenuate the dose rate to enough low level at the outside of the wall. To save unrealistic ceiling thickness of the wide span building, the sky shine can be reduced below trivial level by plating about 1.5 m thick concrete shield just over the tokamak machine with the 50 cm thick ceiling.

(M. Kasai)

5.3 Toroidal Field Coils

5.3.1 Choice of super-conducting magnet

Super-conducting magnets are employed for the toroidal coils of the Plasma Engineering Test Facility (PETF) in order mainly to lower the power rating of the toroidal coil power supply. Even in the JT-60 toroidal coils 360 MW power consumption and 9.3 GJ per shot heat deposit are estimated, so it is necessary to employ super-conducting magnets for toroidal coils of the PETF, of which scale is about twice larger than JT-60 in one dimension. Use of super-conducting magnets seems to be more economical as a whole than that of normaly conducting coils in case that a machine is operated in long duration, even if the cost of super-conducting magnets and helium liquifier and refrigerator, and its running cost are involved.

NbTi is used as super-conducting material because of its higher development level, and is replaced to Nb_3Sn in case that stronger toroidal magnetic field should be required because of deterioration of plasma confinement. Design value of fusion plasma is so decided as to reach self-ignition based on both existing energy confinement scaling laws, i.e. Alcator scaling as $\tau_E \propto n_a^2$ and trapped ion scaling low even in the toroidal field produced by a NbTi super-conducting magnet.

5.3.2 Shape and size of toroidal field coil

Shape and size of the toroidal field coil are shown in Fig. 5.3.1, and such 16 coils form the PETF toroidal field coil system.

Large electromagnetic force acts on high field toroidal field coils, so a shape of minimum stress distribution, so called constant tension, is desirable. When the centering force due to composed electromagnetic hoop force produced by an interaction between toroidal field and current flowing in the toroidal coil is supported by center cylinder and/or surface contact of wedge-shaped inner part of two neighbouring toroidal field coils, a toroidal field coil has a D-shape of which straight part radially inside. This D-shaped toroidal field coil fits to such a tokamak with poloidal magnetic limiters top and bottom of the inside of the plasma as PETF.

Distance between the inner surface of the plasma and the straight part of the inner perimeter of the D-shape toroidal field coil is kept at 1.1 m for effective use the stronger toroidal field, so the radius of the

straight part of the inner perimeter is equal to 3.7 m resulting the toroidal field coil thickness of 0.9 m. The current density of the toroidal field coil averaged at the overall cross section of the coil is kept at 8 A/mm^2. Width of the coil at the round part should be less than 1.5 m in order that sufficient access gap for NBI and evacuating ports can be insured between two neighbouring toroidal field coils.

5.3.3 Field ripple of the toroidal field coils

Ripple of the toroidal magnetic field must be less than 1 % in order that the energy transport due to ripple diffusion is suppressed less than a few MW. Field ripple is estimated according to Eq. 5.3.1 which tends to show a little bit larger value than that is calculated numerically by computer. Therefore the design is made to keep the field ripple calculated by Eq. 5.3.1 at 0.5% which gives a rather severe estimate.

$$\delta(\%) = \frac{1}{2}\left[\frac{1}{(R/R_1)^N-1} + \frac{1}{(R_2/R)^N-1}\right] \times 100 \qquad (5.3.1)$$

The number of toroidal field coils are so decided as to compromise field ripple reduction at the outer plasma surface with maximization of the access gap for NBI and evacuating ports between two neighbouring toroidal field coils, unless the bore of the coil too much enlarged. To devide toroidal coils into too many number in order to attain field ripple reduction in minimum size raises difficulty of construction and repairing of the machine also with extra cost.

Ripple of the toroidal magnetic field at the outer surface of the plasma (R = 8.6 m) is estimated according to Eq. 5.3.1 and is shown in Fig. 5.3.2 by the function of the major radius from the machine axis of the outer side of inner-most turn R_2 (see Fig. 5.3.4). In the figure, the number of coil, N, is used as a parameter. In Fig. 5.3.3, the outside radius of inner-most turn, R_2, and the access gap on the mid-plane between two adjacent coils, d, are shown by the function of the number of toroidal field coils.

Access gap, d, between two neighbouring toroidal field coils should be more than 2 m in order that the NBI port, of which beam line is inclined to the normal of the plasma surface by about 15 degree, can be equipped with side shield for the beam line. As is shown in Fig. 5.3.3, the number of coil must be less than 16 if we hold the field ripple at 0.5 %. Design

is made at 16 toroidal coils to attain minimum bore (design point 1). If we enlarge the bore of the coil a little to $R_2 \simeq 10.25$ m, then field ripple of 0.5 % is attainable only by 14 coils (design point 2), which allows the distance of about 3.2 m between two coils which is by about 60 % larger than the designed case with 16 coils resulting more space for assembling and repairing the PETF by remote handling. Less number of toroidal field coils with a little bit larger radius seem to be more economical than the contrary case, so the former case will be examined in details for future optimization.

5.3.4 Cryogenics

Super-conducting magnets of the PETF toroidal field coils have a size much larger than these produced in the present, and the LCT coils being designed now. Such a large super-conducting coil system inevitably requires a large and high performance liquid helium circulating system. Besides their large size, super-conducting magnets for fusion use have many problems in various heat loads, which include the heat load from the coil supporting structure to stand for large electromagnetic forces.

Heat sources are as follows:

(1) eddy current loss due to magnetic field change,
(2) heat conduction from a central cylinder, supporting rods against lateral force, and other supporting structure,
(3) internal heat generation due to neutrons and γ-rays,
(4) transfer tube loss, which shares a considerable part in case that cryogenic system is located far from PETF, and
(5) pressure loss of the helium pumps.

These heat losses cannot be estimated in the present, because internal structures of the superconducting toroidal field coils are not designed yet.

Heat is removed by pool boiling from NbTi coils, and forced cooling with super critical helium is possibly employed in case of Nb_3Sn with maximum field of either 12T or low.

5.3.5 Future problems

There are some problems remained in the future study as listed bellow.

(1) Analysis of stress distribution along a toroidal field coil and examination of supporting structure in detail.
(2) Design of detailed structure of the coil interior including cryogenics.

(3) Optimization of coil number and coil bore taking space interaction with the components such as neutral beam injectors and pumping system into consideration.

(4) Examination of transportation, setting and exact alignment of the coils.

(5) Examination of winding structure and electrical connection between coils to minimize the extent of the accident when one of the coils faults.

(6) Examination of one-turn voltage insulation method of the central cylinder and liquid helium can, and development of anti-high tension electrical and heat insulator.

(7) Cost evaluation of the super-conducting toroidal field coils including liquid helium circulating system.

(8) Safety analysis of the toroidal field coils and cryogenic system.

(K. Shinya)

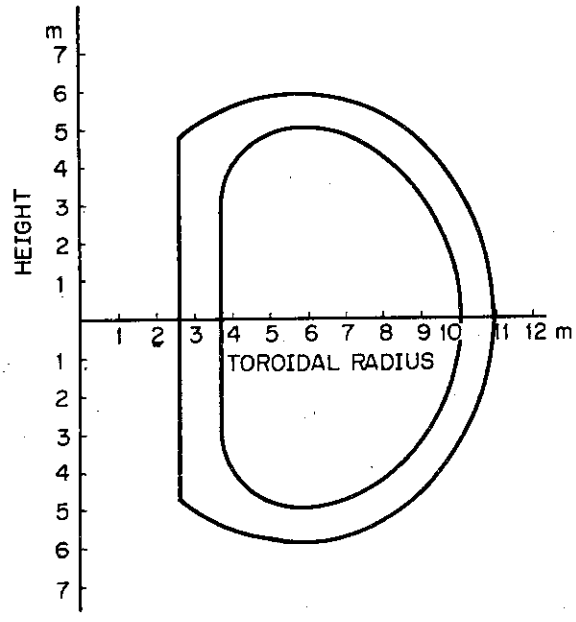

Fig. 5.3.1 Side view of the constant tension toroidal field coil. The field ripple is 0.5 % at the outside plasma surface.

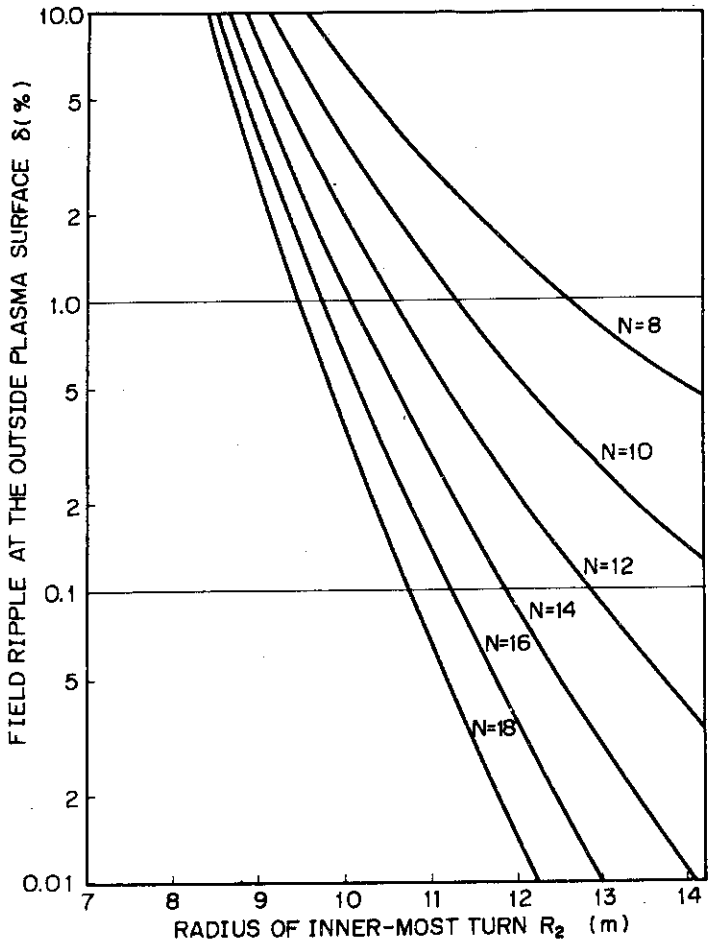

Fig. 5.3.2 Dependence of field ripple on radius of inner-most turn. Parameters are number of toroidal field coils.

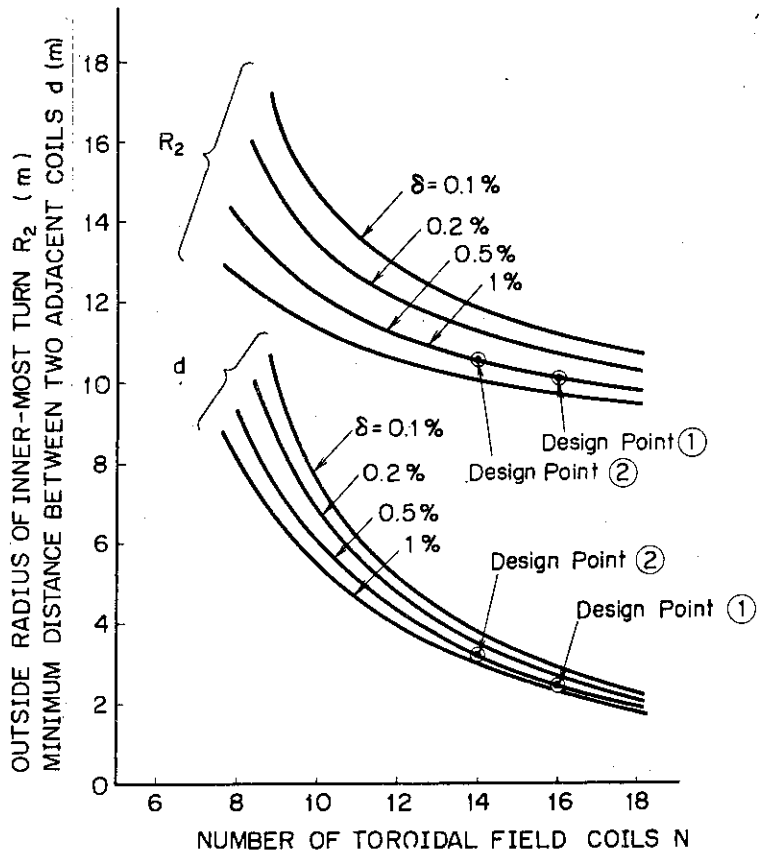

Fig. 5.3.3 Outside radius of the inner-most turn R_2, and the access gap between two adjacent coils d vs number of toroidal field coils, also indicating two design candidate. Parameters are the field ripple at the outside plasma surface.

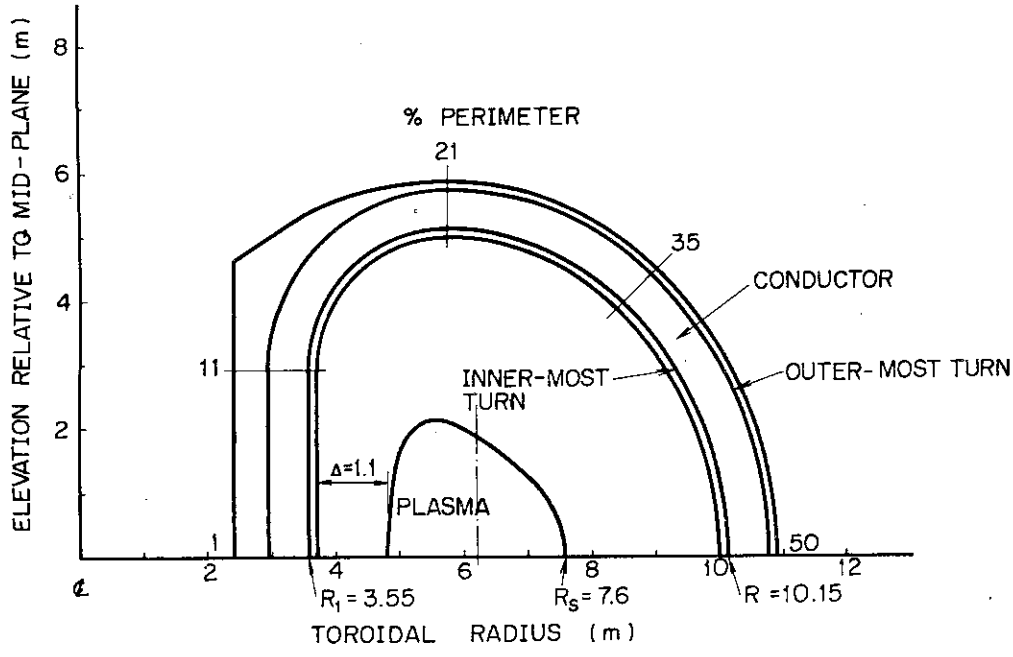

Fig. 5.3.4 Conductor size of the toroidal field coil, also showing the % perimeter

5.4 Poloidal Field Coils

Poloidal field coils is so designed as to ease assembling and repairing the tokamak machine, especially the components placed inside the toroidal field coils, e.g. vacuum vessel, magnetic limiters, radiation shield, etc., unless quality of plasma deteriorated. Guiding principles are

(1) poloidal field coil system placed outside the toroidal field coils, and
(2) reduction of coil number,
(3) with realistic power supply of twice the whole power supply of JT-60 at the maximum.

If poloidal coil system outside the toroidal field coil (outer coil system) is employed, controllability of plasma shape and position is deteriorated resulting requirement for another control or stabilizing coils or their alternatives such as thick conducting shell for fast plasma behaviour inside the toroidal field coils.

For these reason, ohmic heating coils are equipped outside the toroidal coil, and control coils are now being designed in both position, that is, (i) inside the TF-coil (inner coil system) and (ii) outside the TF coil (outer coil system). The latter case oil be possibly employed in the future unless power requirement is into

The number of coils are reduced by adopting hybrid control coil system in which an individual coil has multiple functions, that is, functions producing vertical, quadrupole, and other multipole magnetic fields. Each of the control coils is power-supplied independently.

The overall arrangement of the outer and inner coil system is shown in Fig. 5.4.1 and Fig. 5.4.2 respectively.

5.4.1 Ohmic heating coils

1) Flux change requirement

The total flux change required to excite and to maintain a current of I_p = 4.9 MA in a PETF plasma with R_0 = 6.2 m, a = 1.4 m, κ = 1.5 (ellipticity) and for the maximum burn time T_{BURN} = 60 seconds, is roughly estimated by Eq. 5.4.1,

$$\Phi = L_p I_p + \int R_p I_p \, dt \qquad (5.4.1)$$

where L_p, R_p are inductance and resistance of plasma respectively. Inductance of the PETF plasma, L_p, is calculated for the plasma having

circular cross section with equal poloidal length and uniform current distribution.

Plasma resistance is calculated according to Hazeltine.[1] Current start-up scenario is as follows (see Fig. 5.4.3);

(1) breakdown and ohmic heating phase from t = 0 to 0.5 second up to plasma current of 1 MA, and

(2) the following additional heating phase by neutral beam injection from t = 0.5 to 4 second up to full plasma current of 49 MA.

Flux-change consumed by the plasma resistance is calculated both in current rising phase described above and in the stationary burning phase supposing 60 seconds burning time.

(1) Flux change required for inductive storage of plasma

$$L_p = \mu_o R \ln (8R/a - 7/4) = 12.36 \quad [H]$$

and

$$L_p I_p = 60.54 \quad [v\text{-}s]$$

(2) Resistive loss in the current rising plase

Plasma resistance is assumed to be 1×10^{-6} Ω although this is rather under estimation, and the plasma current is averaged to half the stationary value, i.e., 2.45 MA in this phase

$$\int R_p I_p \, dt \simeq R_p \cdot^{1/2} I_p \cdot T_{rise} = 9.8 \quad [v\text{-}s] .$$

(3) Resistive loss in the stationary burning phase

Plasma resistance is calculated according to Hazeltine, and is 1.8×10^{-3} Ω, flux change required is then $R_p I_p T_{burn} = 5.3$ v-s. Total flux change is the sum of the value calculated above, and is equal to $\Phi = 76$ v-s. Resistive loss in the current-rising phase seems to be rather small, but the control coils are expected to supplement the flux change. After all we decide flux change to be 75 v-s. When Nb_3Sn toroidal field coils are used for the alternative of the NbTi with the maximum magnetic field of 12 T, 112.5 v-s is required.

In order that resistive power loss of ohmic heating coils in the stationary plasma burning can be reduced, currents of the ohmic heating coils are swung in the oposite direction from the value corresponding to half the total volt-second requirement, that is the maximum magnetomotive force of each ohmic heating coil are calculated based on 37.5 v-s flux change.

2) Position of the ohmic heating coils

Ohmic heating coils are placed outside the toroidal field coils for easy assembling and repairing the machine by remote handling, although more power is required for the same flux change as compared with an ohmic heating coil system inside the toroidal field coils. Heat loss in the super-conducting toroidal field coils due to magnetic field change of ohmic heating coils can be remarkably reduced when the ohmic heating coils are placed outside, with an important extra merit of cost-down of toroidal field coils.

The position of each ohmic heating coil should be decided by keeping it off the region of neutral beam injection and exhausting ports, other ports for various plasma observation, and the support structure for toroidal field coils. This forbidden region is also applied to the settlement of the control coils. Furthermore, space should be guaranteed between ohmic heating coils and toroidal field coils against magnetic field leakage of ohmic heating coils.

3) Electrical connection of the ohmic heating coils

Ohmic heating coils are divided into some groups in which coils are connected in series, and these groups are supplied with electric power either in parallel from only one electric power supply, or from several independent power supplies, if necessary.

This method has two advantages described in the following.

(1) Both voltage and current of the electric power supply can be realized simultaneously with the moderate values, even for the large-scale tokamak machine.

(2) Any coil group of the transformer can be used in common with control coils by connecting it to another power supply.

Another candidates are the systems in which (i) all coils are connected in series to single power supply, and or the contrary (ii) all coils are connected in parallel.

JT-60 is a typical example of the former case.[2)]
In this connection power supply tends to increase in voltage to unrealistic value, and the position of each coil must be adjusted quite exactly in order to reduce magnetic field leakage at the plasma region.

The latter has been realized in the serial Doublet machines (including Doublet TNS).[3)] When the coils are connected in parallel, currents are automatically adjusted by mutual inductances, and the exact setting of the

coils are not required. In this case current of the power supply tends to by very high, however, and current interruption seems to be very difficult, if plasma current start-up is done by induced voltage due to interruption of the ohmic heating coil current.

Since this series-parallel connected ohmic heating coils can be flexibly designed by the future analysis without big change of the coil structure, ohmic heating coils are now being designed in the parallel connected coils as a start point to obtain basic data for a design of the PETF. In Table 5.4.1, an example designed in parallel connection corresponding to the coil alignment shown in Fig. 5.4.2 is listed.

The radius of the central solenoid of the transformer coils is 2.0 m, and a support cylinder against a centering force acted by toroidal field coils is placed in the space between this solenoid and the toroidal coils. Magnetic field leaks from the ohmic heating coils by about 10 G at the plasma region which dose not affect the plasma current start-up.

Fig. 5.3.4 shows the difference of the total magneto motive force of ohmic heating coils AT, magnetomotive force per meter AT/m at the solenoid and the magnetic field at the origin B(0) by the function of the radius of the central solenoid for 37.5 v-s flux swing. All three quantities increase with decreasing the radius of the solenoid, so the radius of solenoid should not be decreased further.

5.4.2 Control coil

1) Design principle

Control coil system is designed according to the following principles.

(1) Poloidal magnetic limiters are equipped in the symetrical positions to the mid-plane.

(2) Coils which form a D-shaped plasma in a equilibrium position, are placed outside the toroidal field coils to be assembled and repaired easily by remote handling, and effort is made to reduce the total coil number.

(3) Magnetic limiters are placed outside the vacuum vessel and the sub-coils, which aim at a stabilization of the plasma confined in a separatrix in the vertical direction, are omitted. To stabilize a plasma vertically, conducting shell effect of the plates, which form a slit at the magnetic null point on the separatrix, is expected to suppress plasma motions faster than the frequency of the order of

mill-second. To the slower motions than this frequency, stabilizing coils are used to this end. Stabilizing coils are possibly placed inside the toroidal coils.

(4) Hybrid control coil system, of which indivisual coil has multiple functions such as functions to produce vertical field, a quadrupole field, etc., are adopted to the PETF, so the total magnetomotive forces of the coils summed including their signs need not be reduced to zero. Overall flux change produced by the control coils are expected to act as the supplement of the transformer coils by arranging coils in such positions that the total magnetomotive force nearly equals the opposit value of the plasma current, i.e. $-I_p$.

(5) Electric power rating must be reduced as low as possible.

Coils which inevitably overlap the transformer coils as a result of a design submitted to above design principles are mixed up in the ohmic heating coils to be realized a transformer-control hybrid system.

2) Rough estimation of the magnetomotive forces of the magnetic limiter coils

Poloidal magnetic limiters are equipped in the symmetrical positions with the mid-plane to control impurity contamination of the plasma. Poloidal magnetic limiters also serve as a part of the shaping coils to form a D-shaped plasma.

Magnetic limiter coils are placed outside the vacuum vessel for easy assembly and repairing by remote handling, on the other hand, the null points on the separatrix must be formed inside the vacuum vessel for the impurity control.

To know where a null point exists is important to design hardwares of magnetic limiter. Here we estimate the magnetomotive forces of the magnetic limiter for a given position of the null point and the limiter according to a simplified line current model shown in Fig. 5.4.5(a). On the null point, there exists

$$\frac{I_P}{X_S} + \frac{I_D}{X_D + X_S} - \frac{I_D}{X_D - X_S} = 0 \ . \qquad (5.4.2)$$

If we put $f = I_D/I_p$, then we have

$$\frac{X_S}{X_D} = \frac{1}{1 + 2f^2} \ . \qquad (5.4.3)$$

Provided that Eq. 5.4.3 exists in the case of such a coil arrangement for PETF as is shown in Fig. 5.4.5(b), then we have $f = \sqrt{\frac{1}{2}\left[\left(\frac{X_D}{X_S}\right)^2 - 1\right]} = 0.811$ and $I_p = 3.97$ MA. Magnetic axis is assumed to be displaced radially outside by 0.2 m in the above estimation.

Magnetomotive forces of the other equilibrium control coils are calculated for the cases that I_D nearly equals to 4.0 MAT, and the cases that the electric power can be minimized are serched.

3) Position and magnetomotive force of the control coils

In Fig. 5.4.1, positions of the control coils designed after the principles described before are shown. In this case plasma current, I_p, and poloidal beta, β_p, equal to 4.9 MA and 2.45 respectively. The maximum magnetomotive force of each coil is shown in Table 5.4.2, but these maximum forces are not always loaded simultaneously. All coils are used in common with the transformer coils of which coil numbers are listed in the last column of the table.

An important problem in the design of control coils is to decide which coil system should be inside the toroidal coils or outside for the best fit to the PETF. In the case of coils outside the toroidal coils, great advantage exists in assembling and repairing the PETF by remote handling, but on the contrary larger electric power is required especially for larger multipole field, and controllability of the plasma are deteriorated. Heat deposit in the super-conducting toroidal field coils due to eddy current induced by the magnetic field change is large resulting the necessity of cooling in sophisticated way to avoid large load to the cryogenics.

On the contrary, if the control coils are placed inside the toroidal coils, electric power rating can be lowered, and controllability of the plasma is improved but principle defect exists in this case, that is, coils must be joind in assembling and cut in repairing. Concerning heat deposit due to eddy current in the toroidal coils, control coils are effective on the shielding of the magnetic field produced by the plasma current on an average if the total magnetomotive force summed including the sign of each force nearly equals to the opposite to the plasma current I_p.

No matter how inner control coil system has many advantages as described above, control coils are placed outside because PETF is the machine constructed in the near future, of which D-T plasma burns, and, as a result, easy assembling and reparing by remote handling should be prior to others.

Figure 5.4.6 shows an example of control coil arrangement which seems to be favourable in the present because of its lower total power. Magnetomotive force of each coil and required power are listed in Table 5.4.3. All coils are used in common with ohmic heating coils as is shown in Fig. 5.4.1, and the corresponding coil numbers are shown in the last column in the table.

Figure 5.4.7 shows an example of an alternative coil design which is adopted in case that more space should be required between the null point and the magnetic limiter coils. Total magnetomotive force remains almost constant, but unfortunately, the inductive power increases by 20 % (see Table 5.4.4).

Sub-coils of the magnetic limiter, which act for stabilization of vertical plasma motion, are omitted in these design of control coils, simply because sub-coils cannot be aligned outside the vacuum vessel. The coils inside the vacuum vessel seems to be impossible to be equipped or repaired by remote handling.

Designs were made also in the cases of coils placed inside the toroidal field coils (inner coil system) to compare magnetomotive forces of the coils and the electric power, and is shown in Figs. 5.4.8 and 5.4.9, and Tables 5.4.5 and 5.4.6 for two typical magnetic limiter coil alignment. Electric powers are decreased to 50 % (Fig. 5.4.8) and 40 % (Fig. 5.4.9) compared with the corresponding cases of the same magnetic limiter coil alignment of the outer coil system.

Poloidal magnetic field distribution produced by control coils along the inner-most turn and the outer-most turn of the toroidal field coil is shown in Figs. 5.4.10 and 5.4.11 for the outer and the inner oil system. The maximum field point appears near the No. 2 coil in the outer coil system, and near the No. 1 coil in the inner coil system.

Plasma current produces magnetic field of which parallel component is in the negative direction, resulting decrease of peak value in the inner coil system, and increase in the outer one. Coils inside the toroidal coil produce less magnetic field on an average along the toroidal coil, but the peak value exists in the region of stronger toroidal magnetic field. Therefore there is no remarkable advantage in arranging control coils inside the toroidal coils.

4) Further investigation to be done in the future study

Problems to be investigated in the future design are the following.

(1) Optimization of coil positions and magnetomotive forces by taking account of reduction of electric power, magnetic field along the toroidal coil and lateral force acting on the toroidal coils.

(2) Examination of vertical plasma stability without sub-coils of the magnetic limiter.

(3) Detailed design of each coil; number of turns, current density, cooling method, electrical insulation under the large flux of fast neutrons, etc.

(4) Wxamination of connecting and cutting method of the magnetic limiter coils by remote handling.

(5) Examination of the applicability of split coils to the magnetic limiter.

(K. Shinya)

Table 5.4.1 OHMIC HEATING COIL LOCATIONS AND ELECTRICAL PARAMETERS

COIL NO.	R (m)	Z (m)	CURRENT DENSITY (A/mm^2)	MAGNETOMOTIVE FORCE (MAT)	INDUCTIVE POWER (MW)	JOULE LOSS (MW)	HEAT DEPOSIT (MJ)	NO. OF TURNS
1	2.0	0.5	10.0	2.43	22.81	6.12	366.9	20
2	2.0	1.5	10.0	2,43	22.82	6,12	367.0	20
3	2.0	2.5	10.0	2.43	22.81	6.12	367.0	20
4	2.0	3.5	10.0	2.48	23.28	6.24	374.4	20
5	2.04	4.5	9.79	2.73	25.62	6.87	412.1	20
6	2.35	5.4	8.52	1.89	17.67	4.74	284.2	20
7	2.9	6.14	6.70	1.04	9.75	2.61	156.8	20
8	3.6	6.65	5.56	0.58	5.46	1.46	87.8	20
9	5.1	7.0	4.36	0.62	6.48	1.74	104.2	18
10	7.5	6.66	2.96	0.24	2.45	0.66	39.3	18
11	9.75	5,24	2.41	0.18	2.04	0.55	32.7	17
12	11.25	2.72	2.09	0.11	1.23	0.33	19.7	17
TOTAL				34.35	324.81	87.08	5224.5	460

Total value is the sum of the upper and the lower half plane.

TABLE 5.4.2 POLOIDAL COIL LOCATIONS AND ELECTRIC PARAMETERS (MAXIMUM RATINGS)

COIL NO.	R (m)	Z (m)	NO. OF TURNS	CURRENT DENSITY (A/mm^2)	MAGNETOMOTIVE FORCE (MAT)	INDUCTIVE POWER (MW)	JOULE LOSS (MW)	HEAT DEPOSIT (MJ)	FUNCTION
1	2.0	0.5	20	10.0	±2.5	24.0	6.3	378.0	hybrid
2	2.0	1.5	20	10.0	±2.5	24.0	6.3	378.0	hybrid
3	2.0	2.5	20	10.0	2.5	24.0	6.3	378.0	OH-only
4	2.0	3.5	20	10.0	2.5	24.0	6.3	378.0	OH-only
5	2.04	4.5	20	9.79	2.8	27.0	7.1	426.0	OH-only
6	2.35	5.4	20	8.52	1.9	18.0	4.8	288.0	OH-only
7	2.9	6.14	20	6.70	1.1	11.0	2.8	168.0	OH-only
8	3.6	6.65	20	5.56	0.6	6.0	1.5	90.0	OH-only
9	5.1	7.0	18	4.36	0.7	8.0	2.0	120.0	OH-only
10	7.5	6.66	20	10.0	2.0	59.0	19.0	1140.0	hybrid
11 #1	9.5	5.5	20	10.0	2.5	135.0	31.0	1860.0	hybrid
11 #2	10.0	5.0	20	10.0	2.5	135.0	31.0	1860.0	hybrid
12	11.25	2.71	20	10.0	±1.0	10.0	14.1	846.0	hybrid
13	5.0	3.3	20	10.0	-2.0	20.0	12.6	756.0	ML
14	5.0	3.75	20	10.0	-2.0	20.0	12.6	756.0	ML
TOTAL			596		58.2	1126.0	327.4	19644.0	

Total value is the sum of the upper and the lower half plane.
Total magnetomotive force is the sum of the absolute value.
ML means a magnetic limiter.

Table 5.4.3 CONTROL COIL LOCATIONS AND ELECTRICAL PARAMETERS OF OUTER COIL SYSTEM

COIL NO.	R (m)	Z (m)	MAGNETOMOTIVE FORCE (MAT)	INDUCTIVE POWER (MW)	JOULE LOSS (MW)	HEAT DEPOSIT (MJ)	CORRESPONDING OH-COIL NUMBER
1	2.0	0.5	-3.56	25.02	8.96	357.4	1
2	7.5	6.66	1.97	57.80	18.55	1113.1	10
3	9.75	5.24	4.79	253.76	58.68	3520.5	11
4	11.25	2.71	-0.96	8.33	13.50	809.8	12
5	4.75	3.3	-0.90	8.29	5.37	322.3	ML
6	5.25	3.3	-0.90	7.81	5.94	356.3	ML
7	4.75	3.75	-0.90	7.74	5.37	322.3	ML
8	5.25	3.75	-0.90	7.17	5.94	356.3	ML
TOTAL			29.75	751.85	244.60	14675.8	

Total value is the sum of the upper and the lower half plane.
Total magnetomotive force is the sum of the absolute value.
ML means a magnetic limiter coil.

TABLE 5.4.4 CONTROL COIL LOCATIONS AND ELECTRICAL PARAMETERS OF OUTER COIL SYSTEM
----- ALTERNATIVE MAGNETIC LIMITER PLACED IN PLAIN ------

COIL NO.	R (m)	Z (m)	MAGNETOMOTIVE FORCE (MAT)	INDUCTIVE POWER (MW)	JOULE LOSS (MW)	HEAT DEPOSIT (MJ)	CORRESPONDING OH-COIL NUMBER
1	2.0	0.5	-1.60	5.29	4.02	241.0	1
2	7.5	6.66	5.56	273.27	52.37	3142.5	10
3	9.75	5.24	3.23	167.63	39.62	2377.1	11
4	11.25	2.71	-0.79	10.31	11.15	668.8	12
5	4.5	3.5	-0.90	3.50	5.09	305.4	ML
6	5.0	3.5	-0.90	3.93	5.65	339.3	ML
7	5.5	3.5	-0.90	2.93	6.22	373.2	ML
8	6.0	3.5	-0.90	0.18	6.79	407.2	ML
TOTAL			29.55	938.08	263.87	15832.5	

Total value is the sum of the upper and the lower half plane.
Total magnetomotive force is the sum of the absolute value.
ML means a magnetic limiter coil.

TABLE 5.4.5 CONTROL COIL LOCATIONS AND ELECTRICAL PARAMETERS OF INNER COIL SYSTEM

COIL NO.	R (m)	Z (m)	MAGNETOMOTIVE FORCE (MAT)	INDUCTIVE POWER (MW)	JOULE LOSS (MW)	HEAT DEPOSIT (MJ)	CORRESPONDING OH-COIL NUMBER
1	4.0	1.5	3.40	52.21	17.09	1025.3	none
2	7.0	3.0	1.38	30.43	12.17	730.4	none
3	8.5	2.0	2.23	76.27	23.82	1429.3	none
4	4.75	3.3	-0.90	1.76	5.37	322.3	ML
5	5.25	3.3	-0.90	1.03	5.94	356.3	ML
6	4.75	3.75	-0.90	2.90	5.37	322.3	ML
7	5.25	3.75	-0.90	2.22	5.94	356.3	ML
TOTAL			21.23	333.67	151.40	9084.3	

Total value is the sum of the upper and the lower half plane.
Total magnetomotive force is the sum of the absolute value.
ML means a magnetic limiter coil.

TABLE 5.4.6 CONTROL COIL LOCATIONS AND ELECTRICAL PARAMETERS OF INNER COIL SYSTEM
----- ALTERNATIVE MAGNETIC LIMITER PLACED IN PLAIN -----

COIL NO.	R (m)	Z (m)	MAGNETOMOTIVE FORCE (MAT)	INDUCTIVE POWER (MW)	JOULE LOSS (MW)	HEAT DEPOSIT (MJ)	CORRESPONDING OH-COIL NUMBER
1	4.0	1.5	3.14	46.27	15.80	947.9	none
2	7.0	3.0	1.60	34.67	14.08	844.0	none
3	8.5	2.0	2.21	74.39	23.63	1417.7	none
4	4.5	3.5	-0.90	1.02	4.09	305.4	ML
5	5.0	3.5	-0.90	1.61	5.65	339.3	ML
6	5.5	3.5	-0.90	0.77	6.22	373.2	ML
7	6.0	3.5	-0.90	2.03	6.78	407.2	ML
TOTAL			21.11	321.51	154.51	9270.4	

Total value is the sum of the upper and the lower half plane.
Total magnetomotive force is the sum of the absolute value.
ML means a magnetic limiter coil.

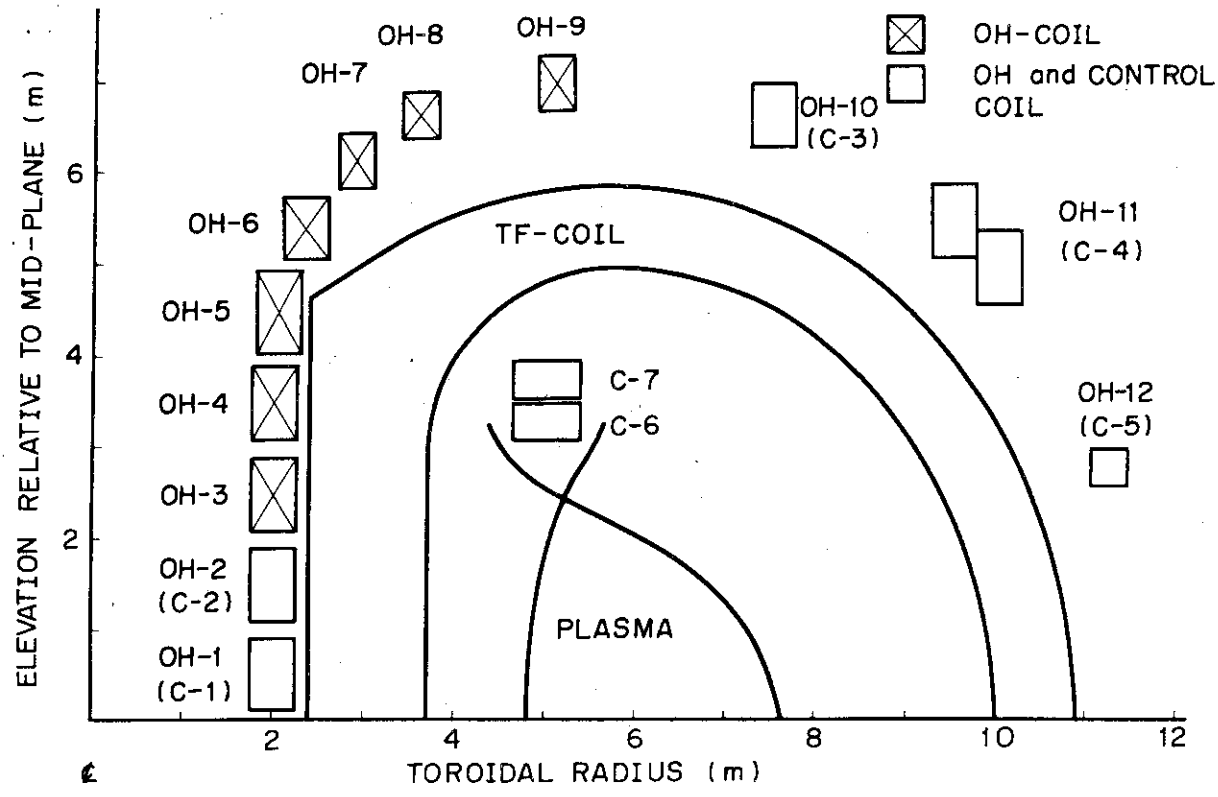

Fig. 5.4.1 Arrangement of the outer poloidal coil system employed in the PETF

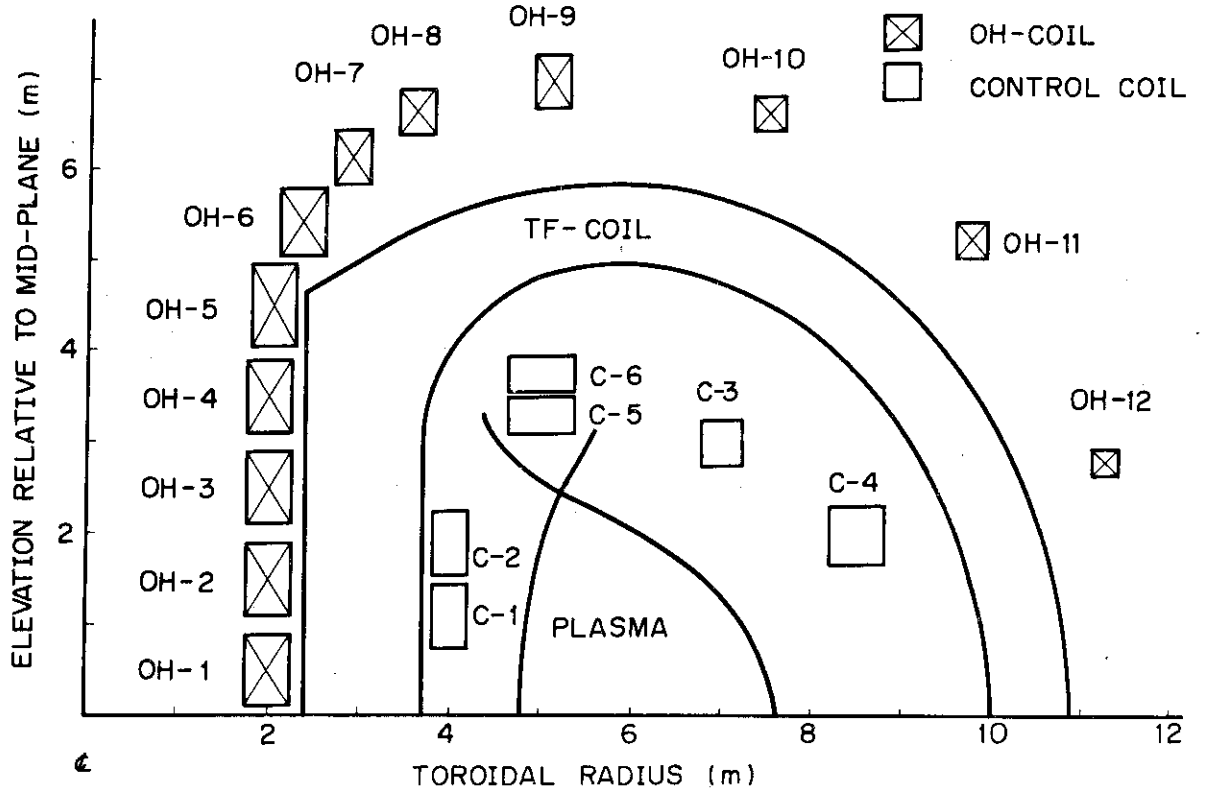

Fig. 5.4.2 Arrangement of the inner poloidal coil system as an alternative

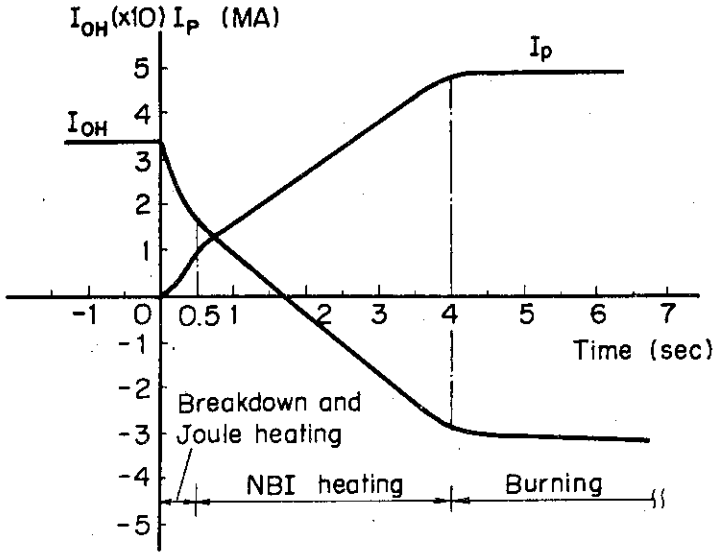

Fig. 5.4.3 Plasma current start-up scenario

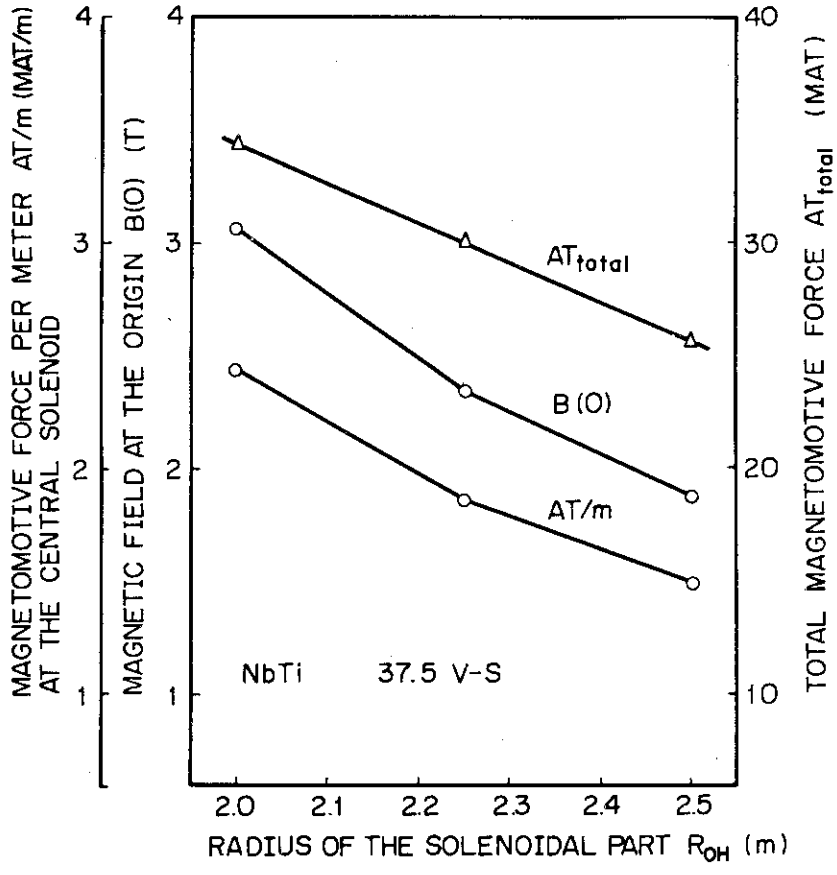

Fig. 5.4.4 Dependence of various parameters of air-core transformer coils on the radius of the solenoidal part of the transformer. Flux change is 37.5 volt-seconds.

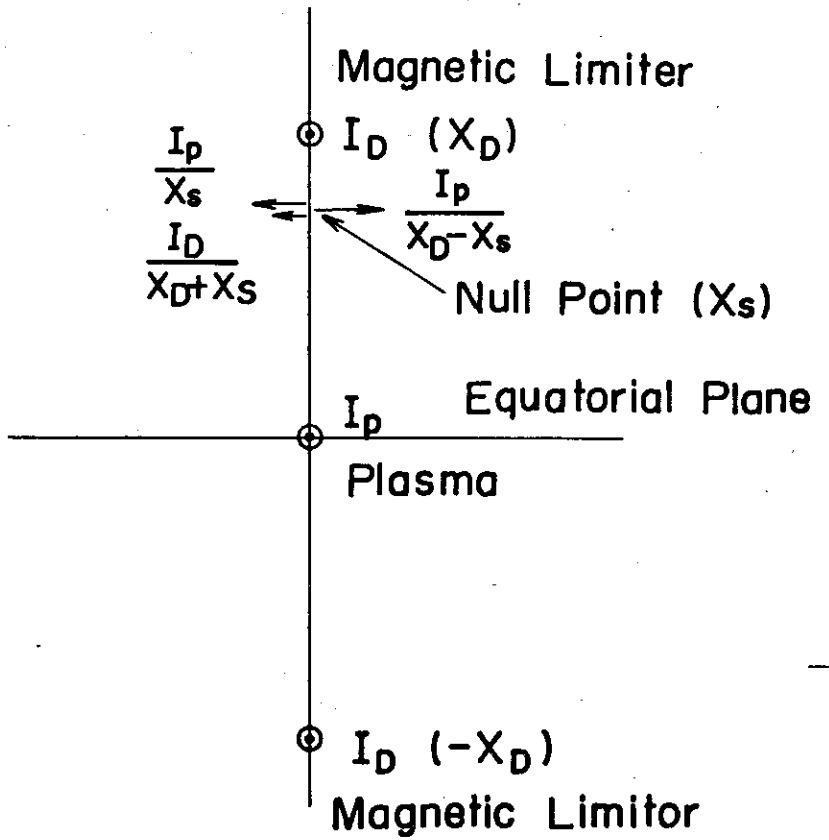

(a) Simplified model for estimation of magnetomotive force of the poloidal magnetic limiter

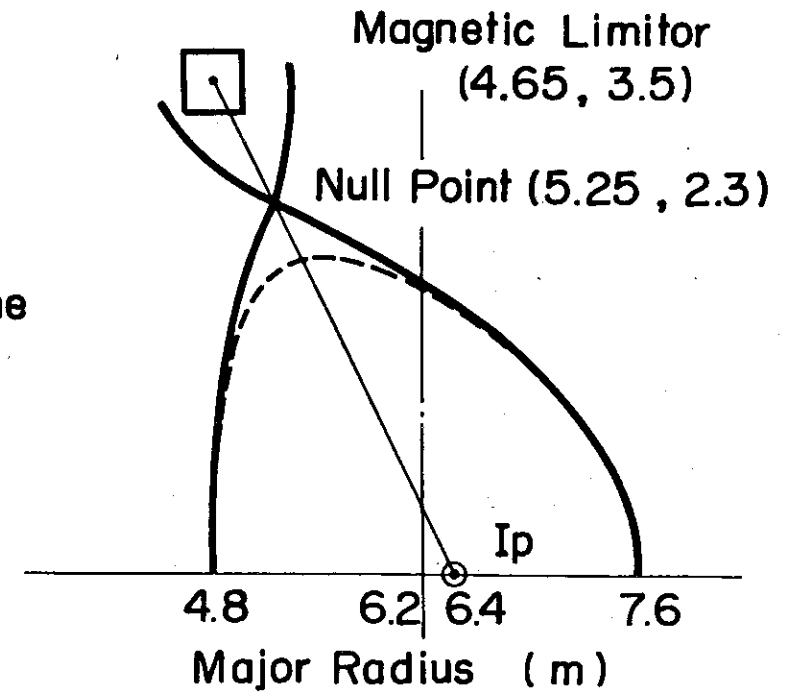

(b) PETF model

Fig. 5.4.5 Models for the calculation of the poloidal magnetic limitor

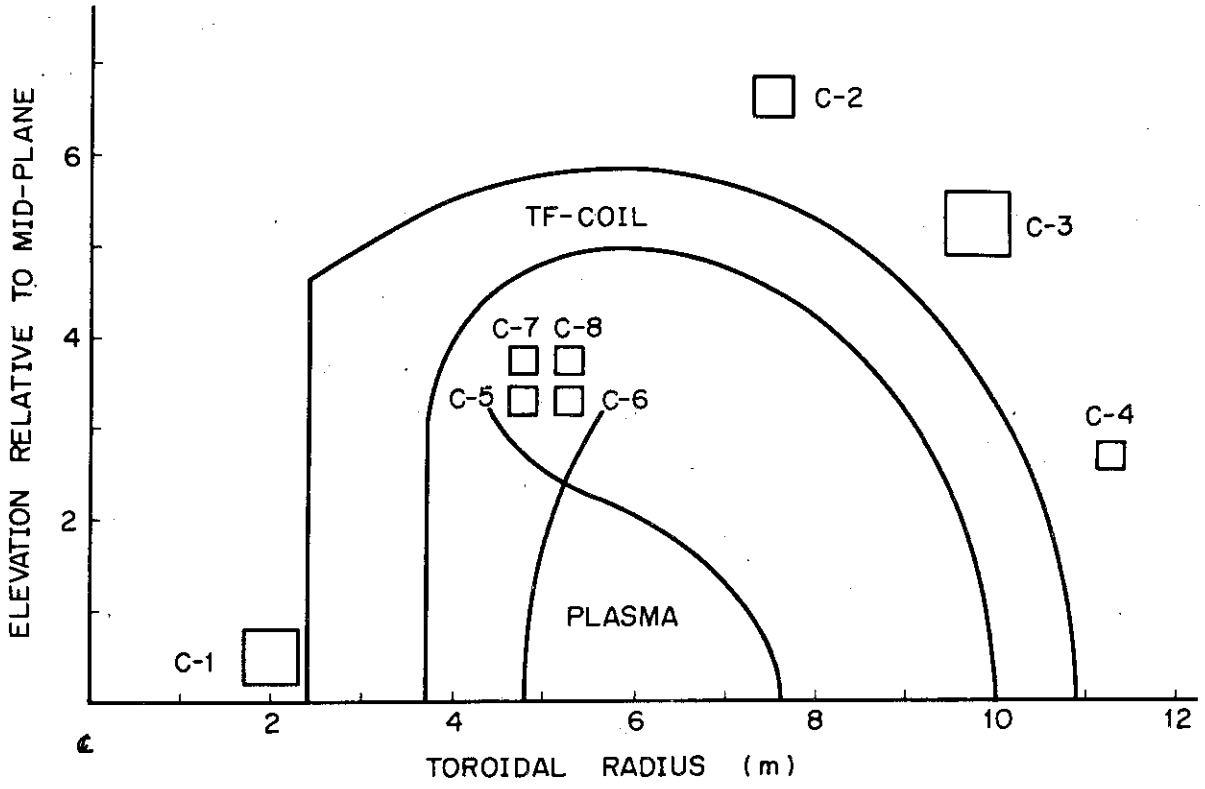

Fig. 5.4.6 An example of the outer control coil system calculated numerically. Size of each coil is calculated with 10 A/mm^2 current density.

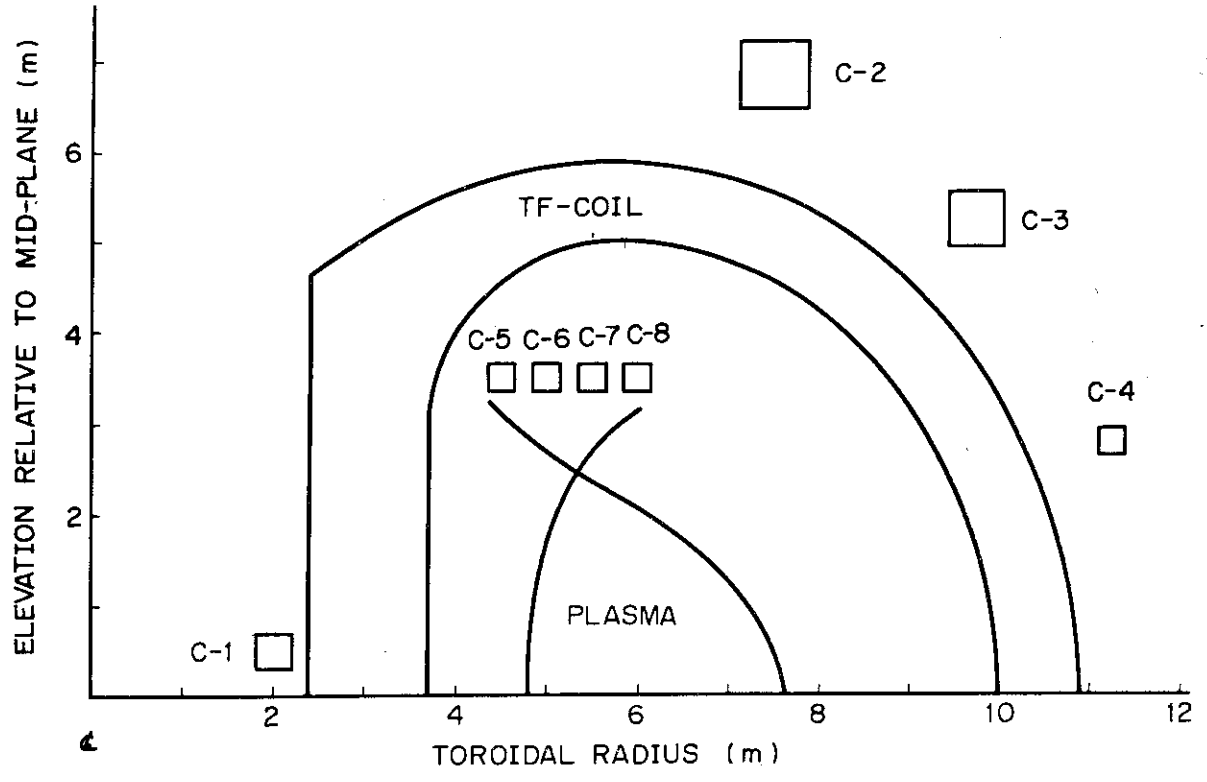

Fig. 5.4.7 An example of the outer control coil system with an alternative magnetic limiter coil placed in plain.

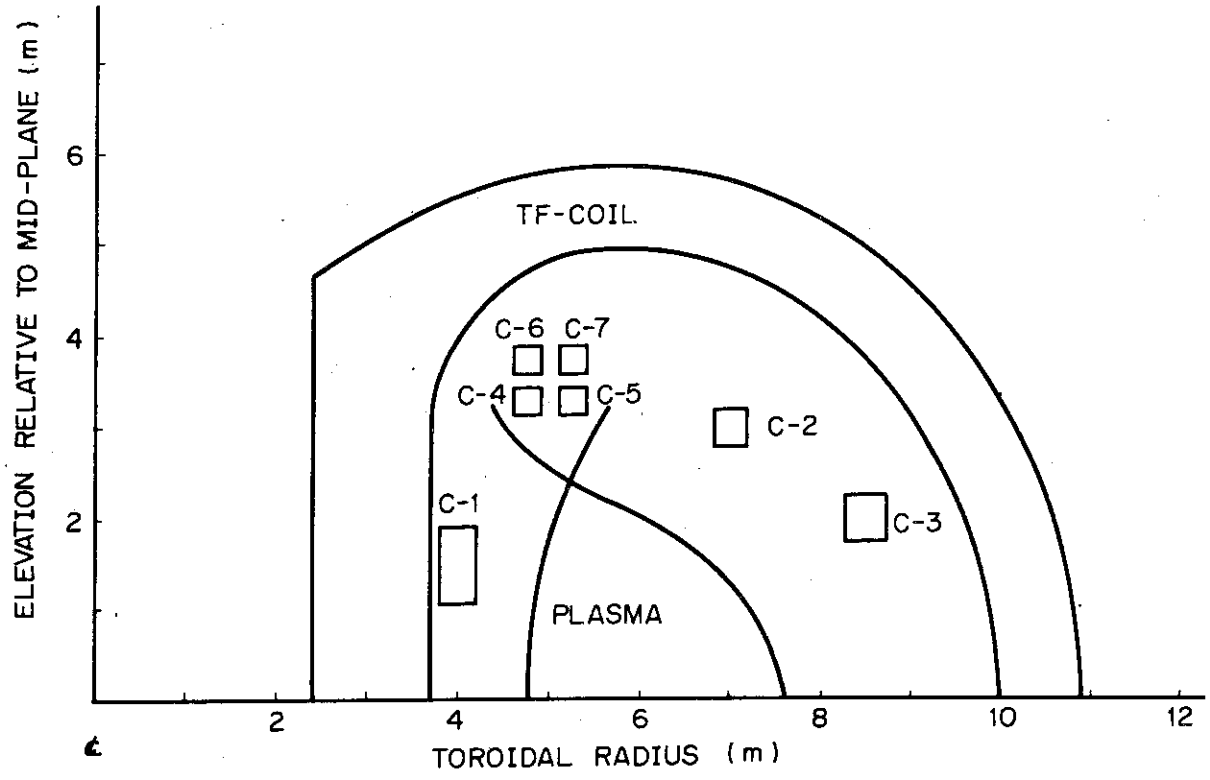

Fig. 5.4.8 An example of the inner control coil system calculated numerically. Size of each coil is calculated with 10 A/mm^2 current density.

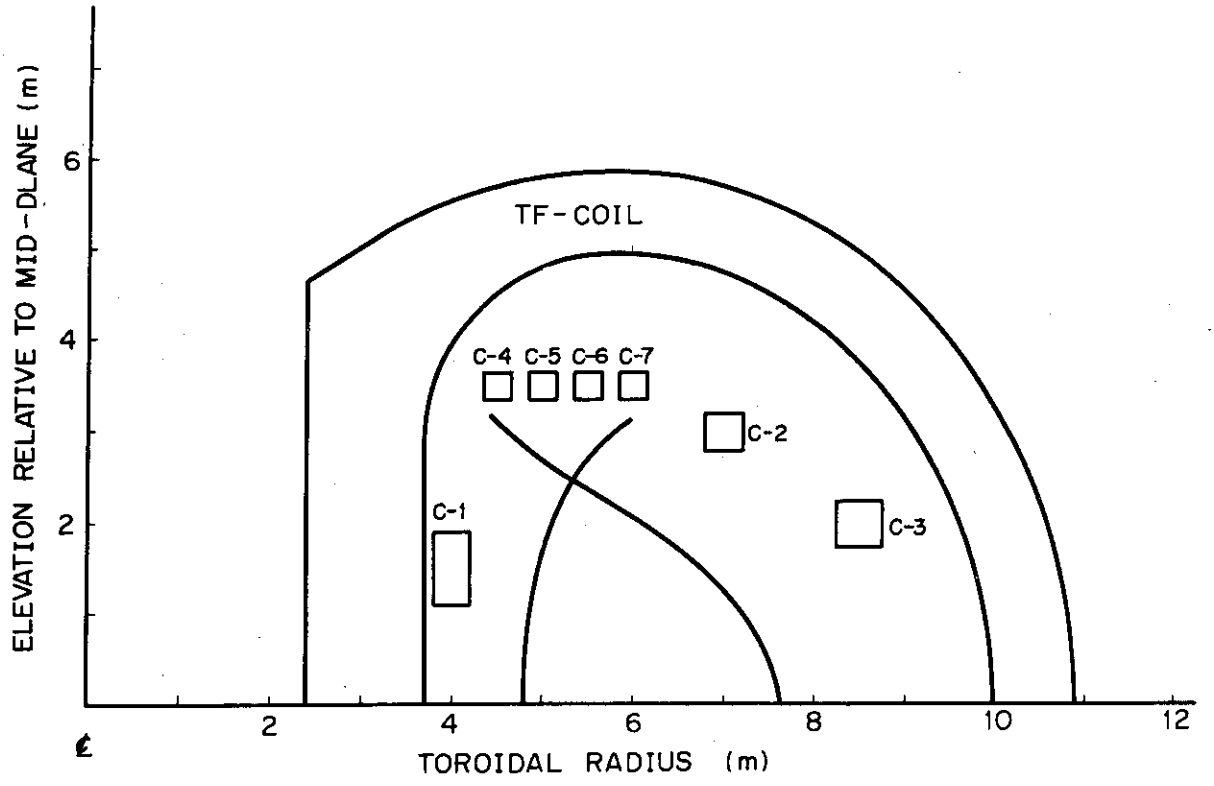

Fig. 5.4.9 An example of the inner control coil system with an alternative magnetic limiter coil placed in plain.

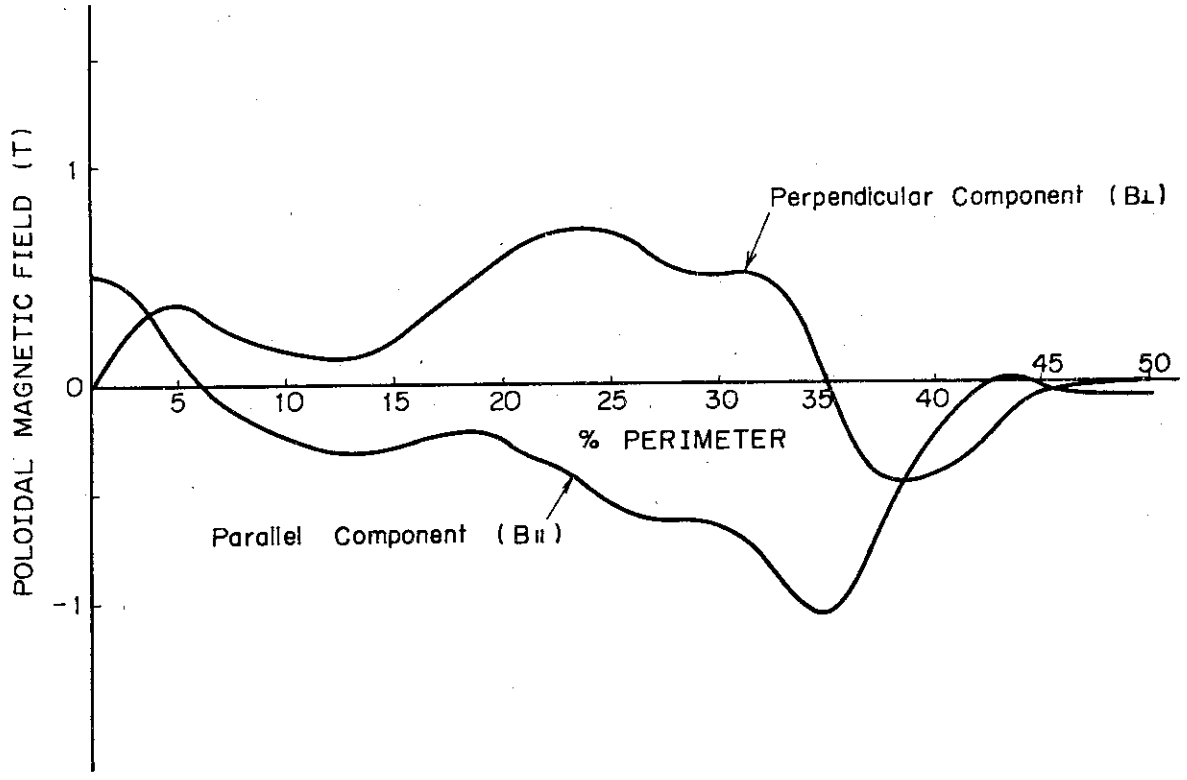

Fig. 5.4.10(a) Poloidal magnetic field profile along the outer-most turn of the toroidal field coil produced by the outer coil system

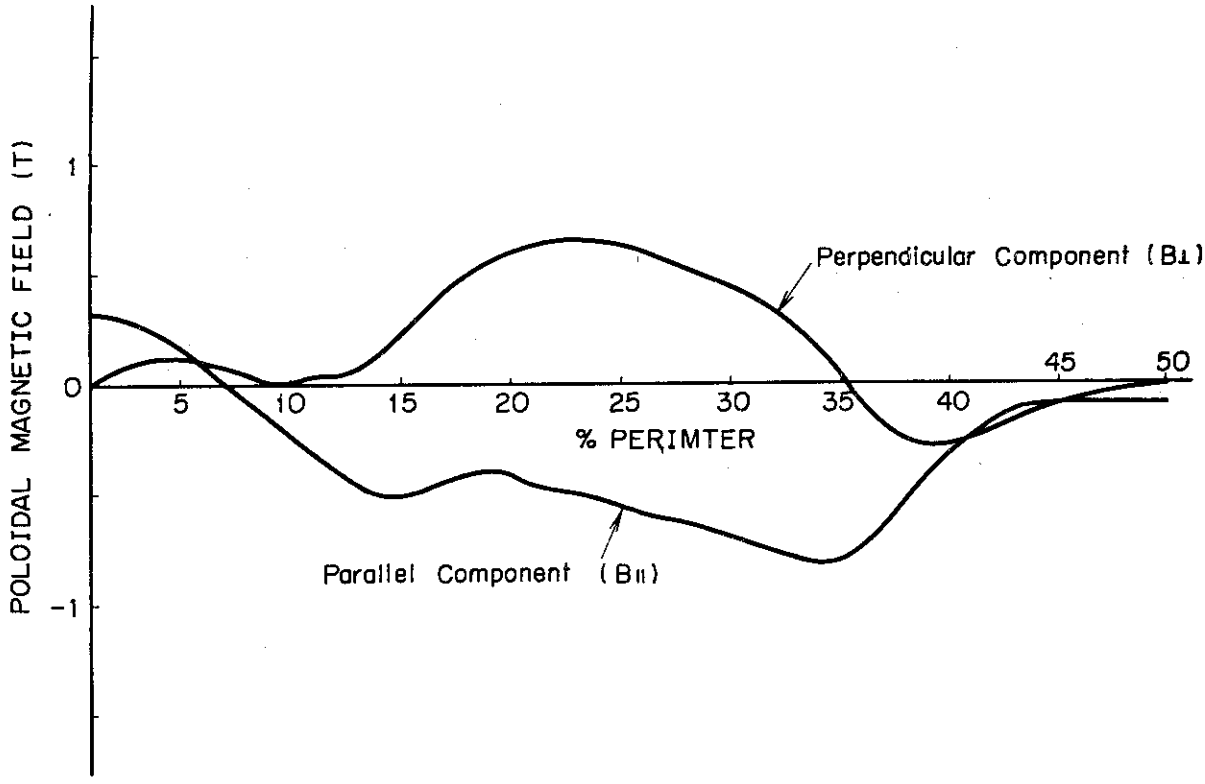

Fig. 5.4.10(b) Poloidal magnetic field profile along the inner-most turn of the toroidal field coil produced by the outer coil system

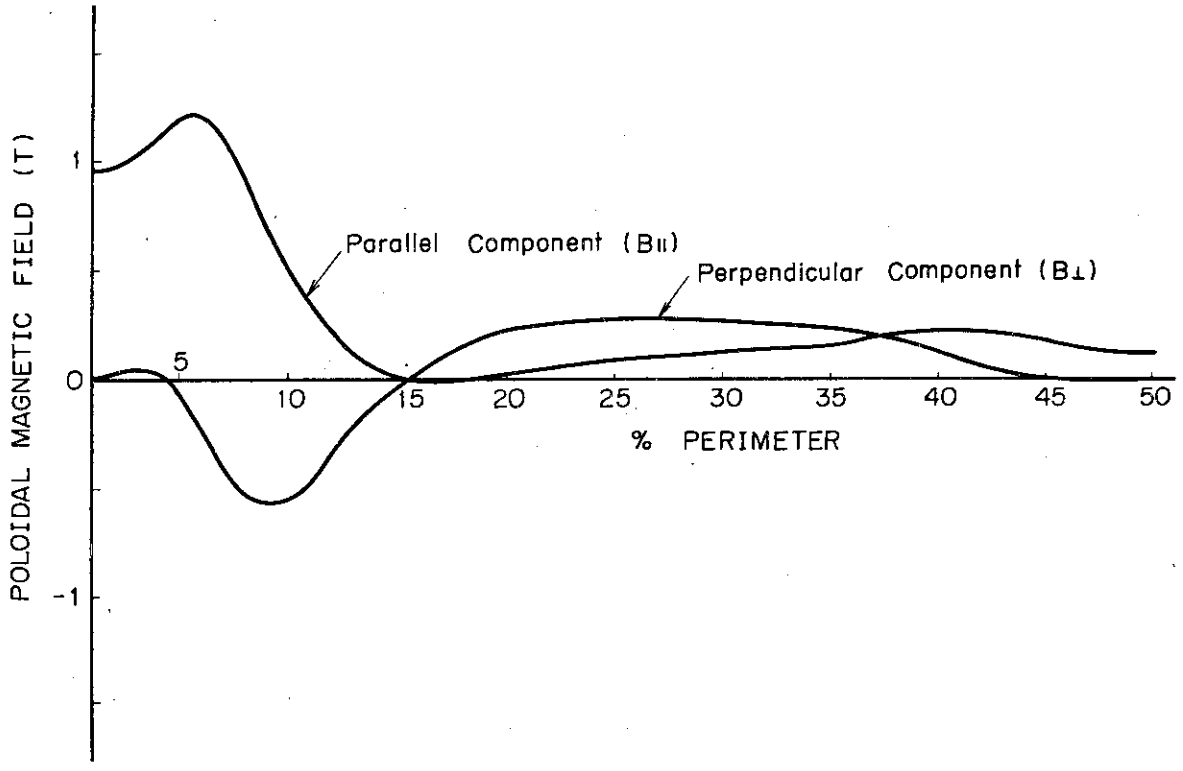

Fig. 5.4.11(a) Poloidal magnetic field profile along the outer-most turn of the toroidal field coil produced by the inner coil system

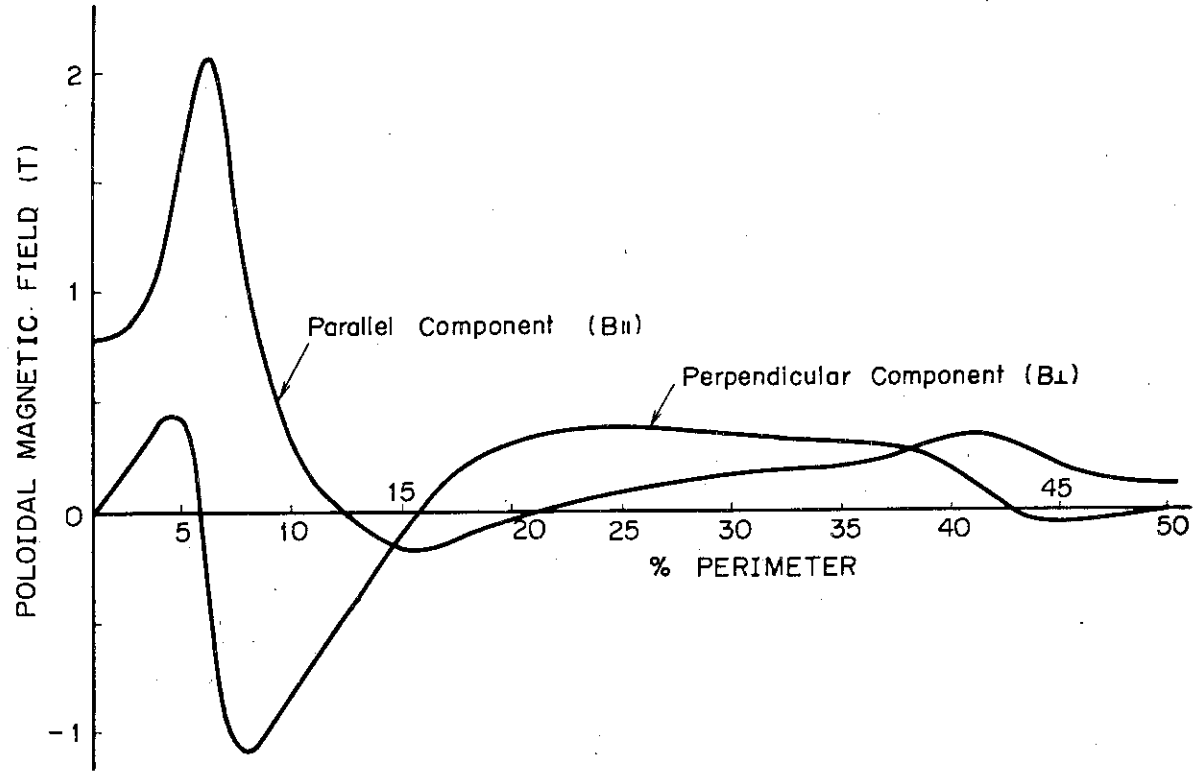

Fig. 5.4.11(b) Poloidal magnetic field profile along the inner-most turn of the toroidal field coil produced by the inner coil system

Reference

1) R. Hazeltine et al.: Physics Fluids 16 (1973) 1675.

2) Y. Suzuki et al.: Proceedings of 5th IAEA Conference on Plasma and Controlled Nuclear Fusion CN-33/A11-2 (1974).

3) W. E. Toffolo et al.: Proceedings of 7th Symposium on Engineering Problems of Fusion Technology 360 (1970).

5.5 Supporting Structure

5.5.1 General description

The supporting structure of PETF forms its framework. It consists of substructure, central part, poloidal field coil support and superstructure. They support following components directly or indirectly.

a) Vacuum vessel
b) Primary shield
c) Toroidal field coil
d) Poloidal field coil
e) Secondary shield

Assembly of eight octant segments around the central part forms the torus of PETF. Each segment is installed on a movable base. It carries octant segments of the vacuum vessel and primary shield with two toroidal coils on the radial transport rails at assembly or disassembly.

The central column sticks on the floor base. The central cylinder also sticks on the floor to sustain the centripetal force by the toroidal field coils. They form the central part of the machine.

The schematic outline of the supporting structure of PETF is shown in Figs. 2.1 and 2.2. It must withstand various kinds of loads such as dead load, electromagnetic foeces, thermal stress, seismic load and others at various kinds of operation conditions.

Most of the supporting structure is made of the high Mn non-magnetic steel whose strength is 1.5 times of SUS304.

Primary shield of PETF is installed in the region between the vacuum vessel and the toroidal field coil. It prevents toroidal field coils from their radiation damage and makes it possible to allow accessibility to the outer periphery of the toroidal coil assembly for easy manual work.

The secondary shield supplements the primary one for biological shielding and it is supported by the superstructure and the peripheral structure of PETF.

5.5.2 Supporting of components

1) Vacuum vessel

The vacuum vessel is hold by the primary shield at its top and bottom positions to make its radial thermal expansion minimum.

The support may have some mechanism to release vertical thermal

expansion. For the vertical movement the similar supports hold the vessel at the equilateral plane.

2) Primary shield

The primary shield works positively as one of the structural components to hold not only the vacuum vessel but some poloidal field coils.

The primary shield itself is supported by its own legs, which stand on the movable base. They suffer very small thermal expansion and will not move the coordinates for the shield and vessel supporting.

The primary shield has 60 cm thickness in the inner portion and 90 cm in the outer portion as shown in Figs. 2.1 and 2.2. Thick casing of stainless steel acts as supporting structure.

3) Toroidal field coil

A couple of toroidal field coils stand directly from the movable base. The hoop tension of each coil sustained by its own casing and reinforcement. The centripetal force by coils are sustained by facing each other lateral sides of the inner wedgeshaped end of a coil and by the central cylinder and the supporting structure between neighboring coils. The supporting structures between neighboring coils also withstand the traverse forces and the vacuum force. The thermal deformation will require some absorption mechanism to the structure.
By the supporting structure between closely aligned coils, the toroidal coil assembly acts actually as one body structure and the only dead load of the coil weight on the movable base.

4) Poloidal field coil

Outer poloidal field coils are held by the supporting structure extended from the movable base and the superstructure as shown in Fig. 2.1. Inner poloidal field coils are supported by the central column. Hoop tensions of all poloidal field coils are sustained by the coils themselves.

The magnetic limiter coils are supported by the primary shield.

5) Secondary shield

Blocks of the secondary shield are supported by the superstructure, the central column and peripheral st ructures. The peripheral structures stand on the movable base.

5.5.3 Secondary shield

The purpose of the secondary shield is biological shielding with the

help of the building walls. It consists of heavy concrete blocks whose thickness is estimated to be about 1.5 meters to reduce the thickness of the ceiling of the building.

5.5.4 Assembly and disassembly procedure

Eight octant segments assembled around the central part form the torus machine of PETF. Each segment is a structure consisting of the vacuum vessel and primary shielding segment and two toroidal coils on the movable base.

The following is the assembly procedure of PETF.

1) Sticking the central column on the floor base
2) Assembly of the blocks of inner poloidal coils around the central column
3) Settlement of the central cylinder with a part of cryostat
4) Assembly of octant segments
   (1) Assembly of movable bases each of which carries a vacuum vessel sector a primary shielding sector and two toroidal coils. The sectors in the toroidal coils were temporally set at a little bit outer position to allow the working space at connection of segments.
   (2) Hlaf four segments of eight are gathered to the center and the inner parts of the cryostat are welded. Then, the sectors of the vacuum vessel and the primary shield are moved to the normal position for connection by welding and bolting.
   (3) The lower poloidal field coils and the limiter coils are inserted and mounted.
   (4) Similar procedure is repeated for a quater with two segments, then, each of octant segment connecting the poloid field coils.
   (5) Supporting structures between segments are mounted.
   (6) The upper poloidal field coils come down from the top and mounted.
   (7) Superstructure is mounted.
   (8) Secondary shield blocks are plated on the superstructure and the peripheral structure.
5) Connection of segments

Sectors of the vacuum vessels and the primary shield are shifted to the normal position after welding works on the inner side. Then, the

vacuum vessel sectors are connected by welding. The primary shield sectors are connected each other by bolting.

6) Connection of poloidal coils

For disassembly, the reverse procedure is traced in principle. However, some components, such as the limiter coils can not help being scrapped.

5.5.5 Problems and R & D requirements

One of the key points for the choice of the assembly procedure is the supporting mechanism of the superconducting toroidal field coil between the room temperature support and the low temperature support. This choice affects the cryostat design and the assembly procedure.

The former allows us very simple assembly of the coil. However, we should endure a large amount of heat loss through the supporting structure because of lack of strong enough superinsulation material withstand the centripetal force, and consequently need high power for the cryogenic system.

The latter is just contrary. Assembly procedure will be very complex because we should weld the inner part of the cryostat.

Thus, the development of the superinsulation material which can withstand the high pressure and strain for the cryostat of the toroidal field coils.

If a reliable ceramic coated metal flange for the vacuum vessel is developed, the structure of the vacuum will gain large flexibility released from the strain of one-turn resistance. It will also provide easier way for assembly and disassembly of the torus.

(H. Sakamoto)

6. Electric Power Supply

6.1 Toroidal Field Coil Power Supply

Toroidal field coils consist of 16 NbTi super-conducting magnets, so power loss due to electrical resistivity is quite small to be neglected, but some power is required for energy storage in the toroidal field coils at the initial excitation of the coils. This forcing power can be small if the coils are forced to be excited slowly enough, for example in two hours.

Toroidal coils of the PETF can be fully excited in about two hours. This excitation duration is so decided as to restrict electric power and voltage to an order of megawatt and hundred volt respectively.

From cryogenic and super-conducting technological points of view, it is realistic that the toroidal coils are supplied with electric power from stabilized current supplies. It seems to be dangerous to short-circuit the coils by using permanent current switches after the coils are fully excited. Therefore, it is probable that power loss in the stabilized current supply exceeds the losses in the coils and the power leads.

Total magnetomotive force AT summed up for 16 coils which are shown in Fig. 5.3.1 is 149 MAT for the maximum toroidal magnetic field of 8 T, and magnetic flux Φ of about 250 Wb is confined in the coils. Hence, the magnetic energy stored in the 16 toroidal field coils is estimated as

$$E_{toroidal} = \frac{1}{2} AT \cdot \Phi = 18.6 \text{ GJ}.$$

If this energy is stored in 2 hours with constant speed as is described above, then the maximum electric power required is

$$P_{toroidal} = 2 \cdot E_{toroidal} / T_{excite} = 5.2 \text{ MW}.$$

This is quite a small fraction of the overall electric power of the PETF.

It should be noticed that much power might be spent in the helium liquifier and refrigerator for toroidal field coil cryogenic system. The cooling load of the toroidal coils is estimated to be an order of 100 kW. About 50 MW electric power is required for the helium liquifier and refrigerator, if 100 kW is deposited to cryogenic temperature, i.e. 4.2 K. This value exceeds by far the initial forcing power.

6.2 Poloidal Field Coil Power Supply

The poloidal field coil power supply of the PETF consists of two parts, that is, the ohmic heating coil (OH-coil) power supply and the control coil power supply.

6.2.1 Ohmic heating coil power supply

Plasma current is excited by swinging the magnetic flux from a corresponding value to half of a required volt-seconds to an equal absolute value with opposite sign. Magnetomotive forces of the ohmic heating coils are changed in the same way. The reason why this method is adopted is to reduce Joule loss in the ohmic heating coils during 60 seconds plasma burning.

Steep current change of the ohmic heating coils during breakdown of the gas and initial rise of a plasma current are induced by interrupting a coil current followed by fast connecting to another high current power supply. Detailed examination of power feed is made in the future study. Homopolar generator may be also taken into consideration, which is suitable to supply high current with low voltage during 60 seconds plasma burning.

The ohmic heating coils are divided into some groups in which individual coils are connected in series, and some of these groups are supplied with electric power by single power supply by connecting them in parallel, and others, which are used in common with control coils, are supplied by another supplies independenty. The maximum magnetomotive forces of the coils, in the case of all of which a connected in parallel, are listed in Table 6.1 corresponding 37.5 v-s flux change, and the position of the coils are shown in Fig. 5.4.2 in the preceeding chapter.

Energy stored in the ohmic heating coil is

$$E_{OH} = \frac{1}{2} AT_i \cdot \Phi_i = 650 \text{ MJ} \quad ,$$

where AT_i and Φ_i denote the magnetomotive force and the magnetic flux linkage of i'th coil. When plasma current is excited linearly in four seconds, the maximum electric forcing power is

$$P_{OH} = 2 E_{OH} / T_{rise} = 325 \text{ MW} \quad ,$$

which is almost comparable to the power of the JT-60 toroidal field coil

power supply. To excite plasma current more quickly demands more electric power, and results realization of the construction of the PETF far away. Therefore, it is desirable to establish a excellent method to excite plasma current as slow as possible.

Joule loss due to electrical resistivity and heat deposit in the coils during one 60 seconds plasma burn are listed in 7'th and last column of Table 6.1, which correspond to the maximum current density of the coil of 10 A/mm^2, current densities differ from each other due to resistive voltage drop equalization in all coils. Total Joule loss and heat deposit are 87 MW and 5.2 GJ/shot respectively. Heat deposit is about a half of that of JT-60 toroidal coils (9.3 GJ/shot), and then there is no benefit in realization of superconducting ohmic heating coils.

6.2.2 Control coil power supply

Each oil has its own power supply and its magnetomotive force is controlled independently since each coil has multiple functions. Position and cross-section of the plasma do not always stay constant as plasma current grows up. Moreover, the final poloidal beta and cross section differ depending on various discharge scheme. Hence, sufficient controllability must be given to the power supply, although stabilization of the plasma for the fast motion by using these coils are unexpectable.

Forcing power during 4-seconds plasma current excitation with the coil alignment shown in Fig. 5.4.6 is estimated at 750 MW (see Table 6.2), which is almost minimum for the designed control coil arrangement. The maximum resistive loss at the current maximum is 250 MW, which corresponds to the 10 A/mm^2 current density of control coils. Heat deposit in the coils during one operation is estimated 14.7 GJ, which is far beyond that of ohmic coils.

In table 6.3 are listed the magnetomotive forces and other quantities of an example of the inner coil system of which coil arrangement is shown in Fig. 5.4.8 in the preceeding chapter. In this arrangement, their positions and magnetomotive forces of the magnetic limiters remains uncharged. In this case, the total magnetomotive force reduces to about 80 % of the outer coil system, and forcing power does 40 %. It is very advantageous to set control coils inside the toroidal coil if the tokamak machine can be assembled and repaired easily by remote handling.

Flux change produced by the control coils at the major radius of the

plasma is estimated at 6.7 v-s in the outer coil system and 65.7 v-s in the inner one. Hence control coils can supplement the flux change of the ohmic heating coils.

In Fig. 6.1 is shown dependence of the total magnetomotive force, the inductive power and the total power of the control coils on the magnetomotive force of one poloidal magnetic limiter located at the position as shown in Fig. 5.4.6. The minimum inductive power exists at the magnetomotive force of the magnetic limiter around 3.6 MA, and the minimum value is estimated at about 750 MW. Null point on the separatrix never exists inside the vacuum vessel if the magnetomotive force of the magnetic limiter is decreased too little.

Magnetomotive force of the No. 1 coil changes its sign from positive to negative (same as magnetic limiter) with increasing the absolute magnetomotive force of the magnetic limiter. No. 1 coil can be omitted by properly setting the magnetomotive force of the magnetic limiter, but from the controllability point of view, this coil can never be omitted, and the power supply for this coil must be able to let current flow in both direction.

6.2.3 Total power of the poloidal field coils

Total power of the poloidal field coils is summarized in Table 6.4. The poloidal coil system of PETF can be realized by almost twice the power and the available energy of JT-60's toroidal and ploidal field coils.[1)]

(K. Shinya)

TABLE 6.1 SUMMARY OF TOTAL ELECTRICAL PARAMETERS

	OH-COIL	OUTER COIL	OUTER COIL (ALTERNATIVE ML)	INNER COIL	INNER COIL (ALTERNATIVE ML)
MAGNETOMOTIVE FORCE (MAT)	34.4	29.8	29.6	21.2	21.1
INDUCTIVE POWER (MW)	328.4	751.9	938.1	333.7	321.5
JOULE LOSS (MW)	89.1	244.6	263.9	151.4	154.5
HEAT DEPOSIT (MJ)	5.2	14.7	15.8	9.1	9.3
CORRESPONDING FIGURE	Fig. 5.4.6	Fig. 5.4.7	Fig. 5.4.8	Fig. 5.4.8	Fig. 5.4.9

With 10 A/mm^2 current density.

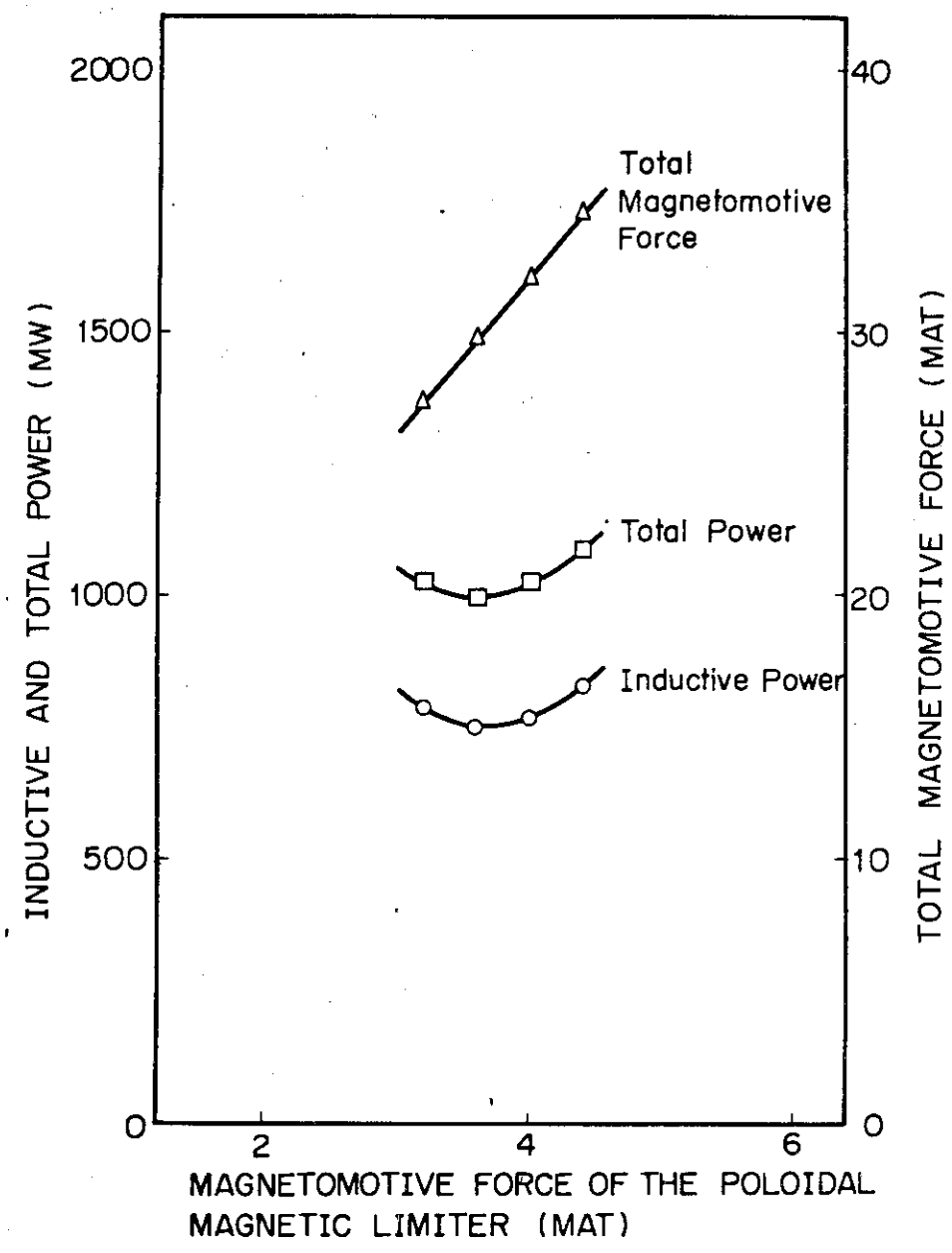

Fig. 6.1 Dependence of power and total magnetomotive force on the magnetomotive force of the magnetic limiter

Reference

1) The JT-60 Power Supply System; IEA Workshop on Power Supplies for Large Tokamaks (1978).

7. Plasma Heating Systems

7.1 Choice of Neutral Beam Injection Heating

The next step large tokamak aiming at a self-ignition demands additional heating power ranging from 50 to 100 MW after ohmic heating. Energetic particle injection (NBI) and absorption of electromagnetic waves excited by external antena (RF) are the reliable candidates to attain these high power heating.

Up to now, there exists more promising experimental results in NBI heating. Also, the physical mechanism by NBI heating is simpler and clearer than that by RF heating. It enables us to design additional heating system of PETF by using neutral beam injection in spite of the attractive mechanical simplicity when RF is employed.

The most important component of the NBI system is the ion source. PETF has a plasma thickness n_a of 2.25×10^{20} atom$\cdot$m^{-2} which requires neutral beam injector to accelerate deuterium beams up to 200 keV to avoid surface heating of the plasma. Neutralization efficiency for a 200 keV deuterium ion beam falls to about 20 per cent as shown in Fig. 7.1[1] resulting in remarkable decrease in overall efficiency of the injection system.

Negative deuterium ion beams can be neutralized by more than 60 per cent, and the value remains almost constant for particle energies above 200 keV. It is advantageous to employ negative ion sources from the view point of the neutralization efficiency, but large current negative ion sources are hardly developed in the present. Therefore, positive ion sources are used for the injector of the Plasma Engineering Test Facility.

7.2 Rough Estimation of the Design Parameters of the Neutral Beam Injector

The neutral beam of 50 MW, 200 keV deuterium is injected in to the torus through eight injection ports corresponding to the half number of the toroidal field coils. Four beamlines are focused on the same injection port of 500 by 1000 mm cross section with its long dimension vertical, which fits to narrow space between two adjacent toroidal coils. One ion source is equipped on each beamline.

Total extraction current from the ion sources can be estimated at 1700 A assuming overall current efficiency of 15 per cent, where the efficiency is defined by the rate of neutral beam current injected into the

plasma to ion current extracted from the ion sources. It seems to be appropriate to extract 50 A ion current from one ion source in the PETF's NBI design resulting that four ion sources are mounted on one injection unit as described above.

The maximum current dnesity of an extracted ion beam is limited by the tolerable heat load into the acceleration electrodes of the ion source, and is roughly estimated at 0.1 A/cm^2 for 200 kV acceleration voltage. If 1 per cent of the beam power are scattered into the acceleration electrodes with equal surface area to the beam cross section, which is very probable in the ion sources, heat flux into the electrodes reaches 200 W/cm^2 which is almost maximum that can be technologically removed. Cross section of the injection port for above current density nearly equals to 5×10^3 cm^2 assuming 40 per cent transparency of the extraction electrodes and twice beam expansion in one dimension, if 4 beam lines are focused on the same port.

The maximum overall power efficiency of the NBI system are optimistically estimated at 30 per cent, even if the remaining ion beam energy can be recovered effectively by the direct energy convertor. Hence, the NBI system of PETF requires electric power for more than 170 MW excluding the power required for the cryo-pumping system.

(K. Shinya)

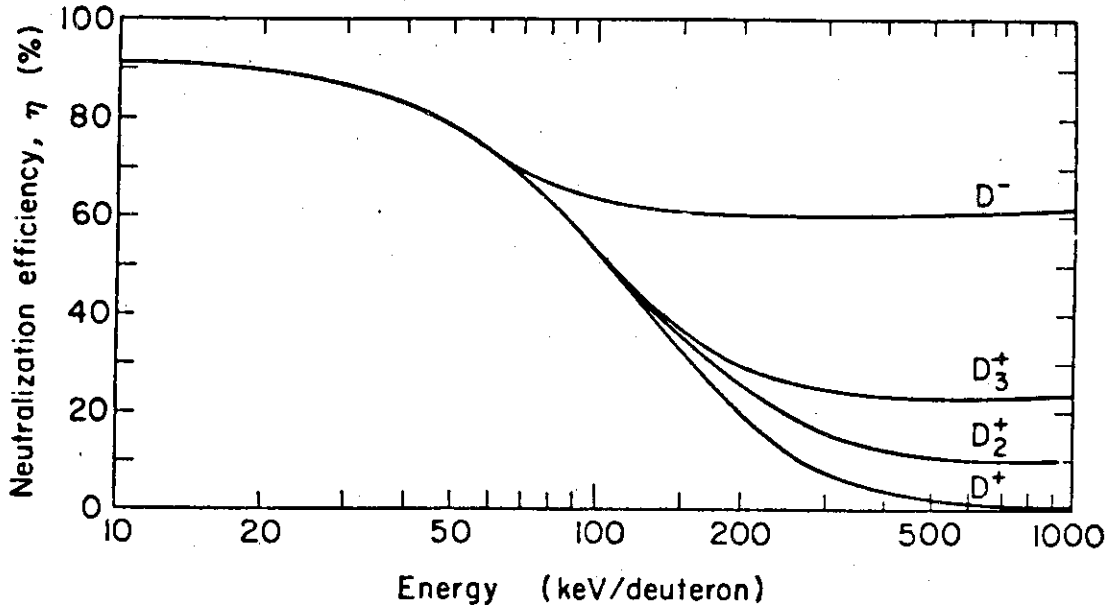

Fig. 7.1 Maximum neutralization efficiency in D_2 vs beam energy, for each of the four beams, D^+, $D^{1/2}$, $D^{1/3}$, and D^- [1]

Reference

1) K. H. Berkner et al.: Proceedings of 1st Topical Meeting on Technology of Controlled Nuclear Fusion C_NF-740402-P1 392 (1974).

8. Tritium System and Inventory

Two kinds of tritium systems are schematically shown in Figs. 8.1 and 8.2. They mainly consist of vacuum pumps, fuel purifier, isotope separation system, tritium storage and fuel injector. One of them adopts cryogenic systems for fuel purifier and for isotope separation system, while the other Pd-Ag diffusers for these systems. The cryogenic system makes tritium leakage from the tritium system minimum at normal operation. On the other hand, the Pd-Ag diffuser makes the tritium inventory in the tritium system minimum, which will minimize tritium leakage at failure. However, it requires the reliable containment system of tritium at normal operation because of its high operating temperature.

Initial tritium inventories in PETF required to start up and operate PETF for one year are estimated for the two tritium systems mentioned in the above. They are summarized in Table 8.1.

The estimated initial tritium inventory will be 190 ∿ 200 g. These tritium inventories are estimated for the following conditions.

a) PETF is operated 40 shots/day and 200 days/year.

b) The amount of tritium filling gas and consumption by 30 second burning per shot are 0.15 g and 0.015 g respectively.

c) Vacuum pumps and the input tank No. 1 have a capacity for the amount of the exhausted tritium for 5 days.

d) The holding capacity of the input tank No. 2 (surge tank) is for the amount of tritium for one day.

e) The exhausted gas from NBI system is treated together with that from the plasma chamber.

f) The amount of tritium consumed in one year should be initially stored in tritium storage.

Thus, the initial inventory for PETF is 200 g with some margin.

(M. Kasai)

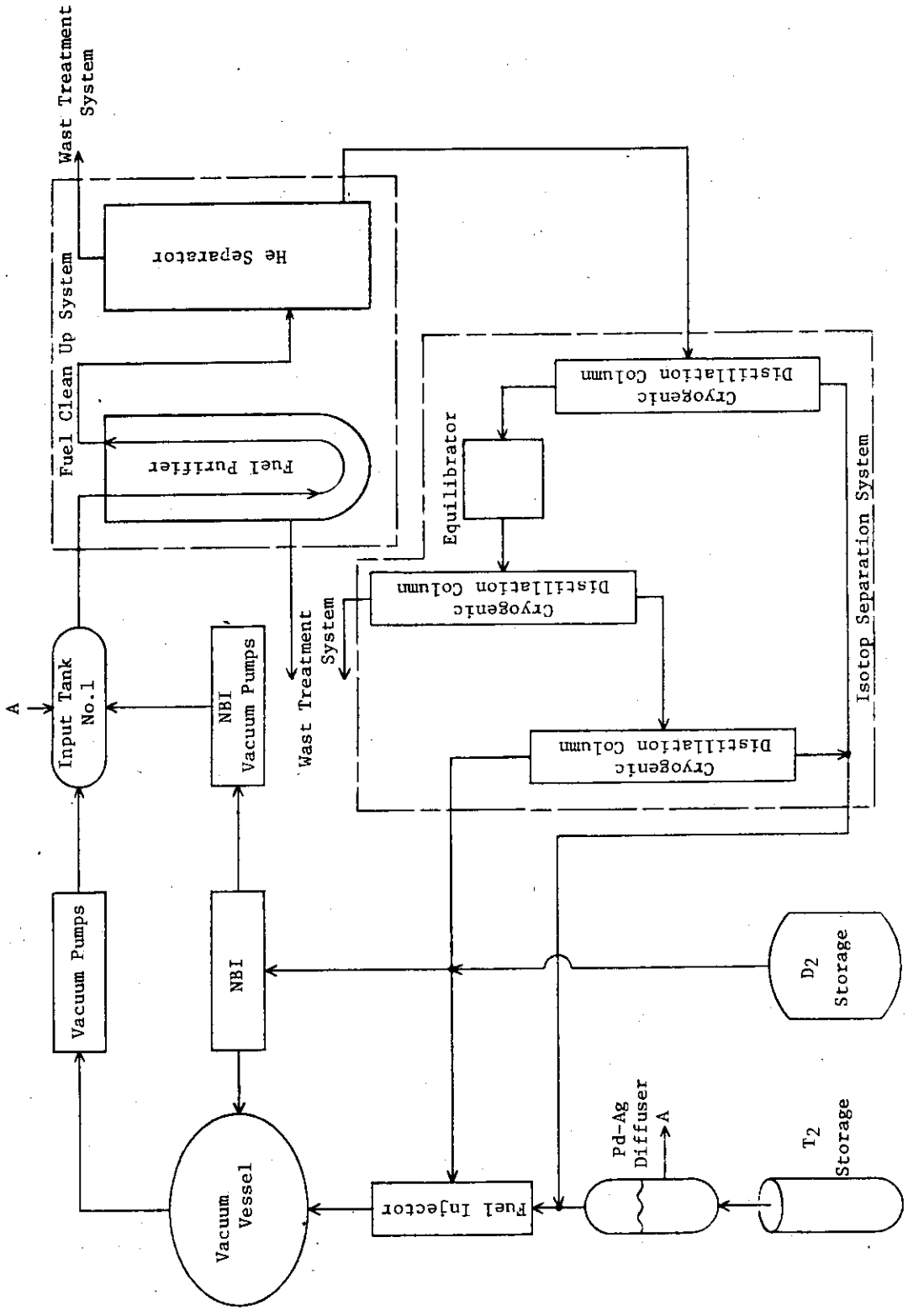

Fig. 8.1 Schematic diagram of cryogenic tritium system

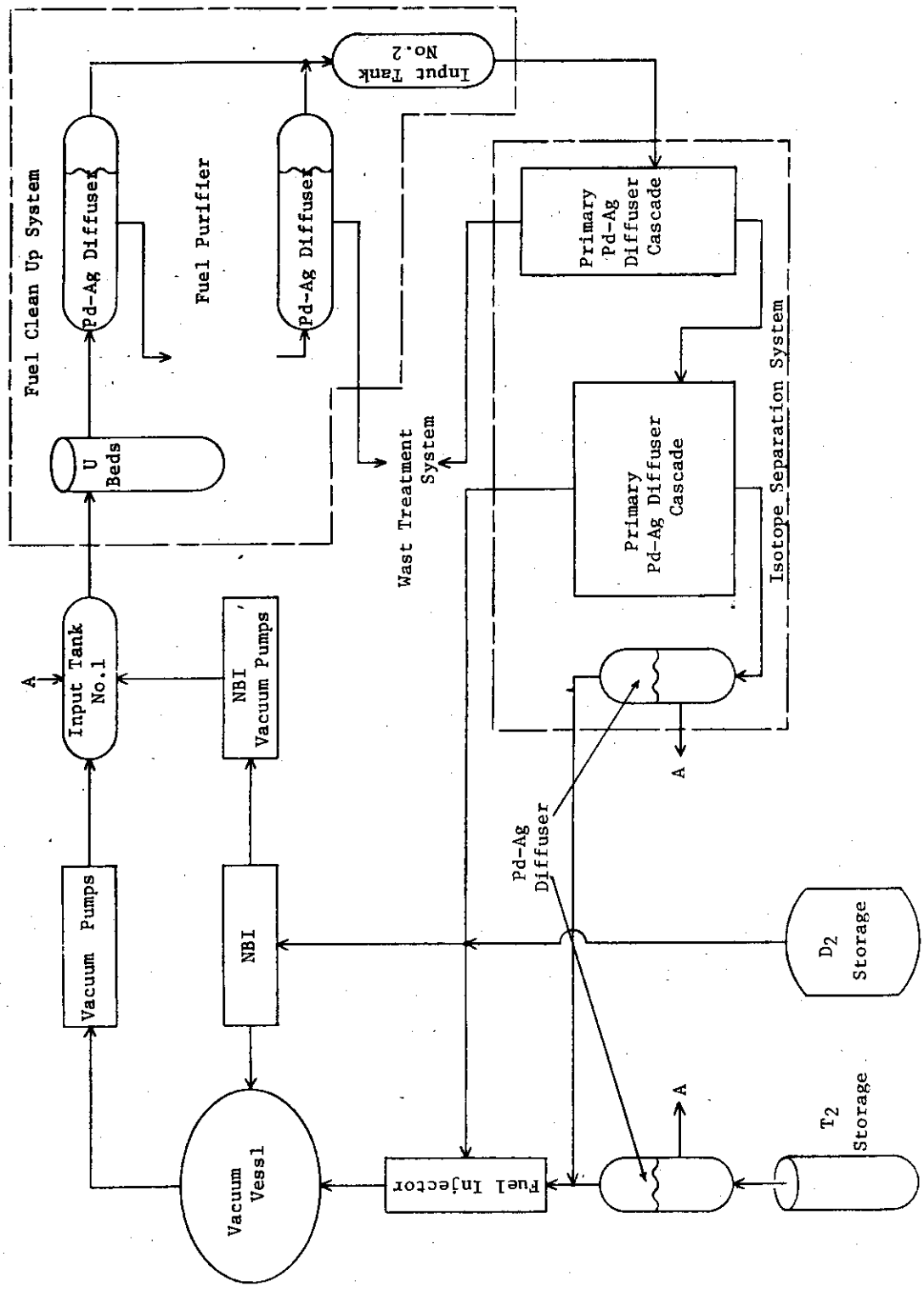

Fig. 8.2 Schematic diagram of Pd-Ag diffuser tritium system

TABLE 8.1 TRITIUM INVENTORIES IN PETF

	Cryogentic System	Pd-Ag Diffuser
Vacuum Pumps & Input Tunk No. 1	30 g	30 g
Fuel Clean Up System*	1 g	8 g
Isotope Separation System	30 g	15 g
Fuel Injector	6 g	6 g
T_2 Storage	120 g	120 g
T_2 Decay	10 g	10 g
Total	197 g	189 g

* Fuel clean up system consists of U beds, fuel purifier and input tank No. 2 (surge tank) in the case of Pd-Ag diffuser.

Acknowledgement

Authors sincerely acknowledge Drs. S. Mori, Y. Iso and M. Yoshikawa for their heartful encouragement. They also thank deeply Mr. Y. Matsuda for his contribution to the discussions on the tritium system. They express their gratitude to

H. Iida
H. Kishimoto
H. Takatsu
H. Tsuji

as members of PETF Study Meeting and

N. Fujisawa
S. Matsuda
T. Nagashima
S. Seki
Y. Shimomura
T. Tone
T. Tuda

as member of Plasma Steering Meeting for their discussions and comments.

Authors would like to adknowledge deeply to Mitsubishi Group, Toshiba Co., Ltd. and Hitachi, Ltd. for their contribution through the concept study of PETF.